Article

Cancer Cell

A niche driven mechanism determines response and a mutation-independent therapeutic approach for myeloid malignancies

Graphical abstract

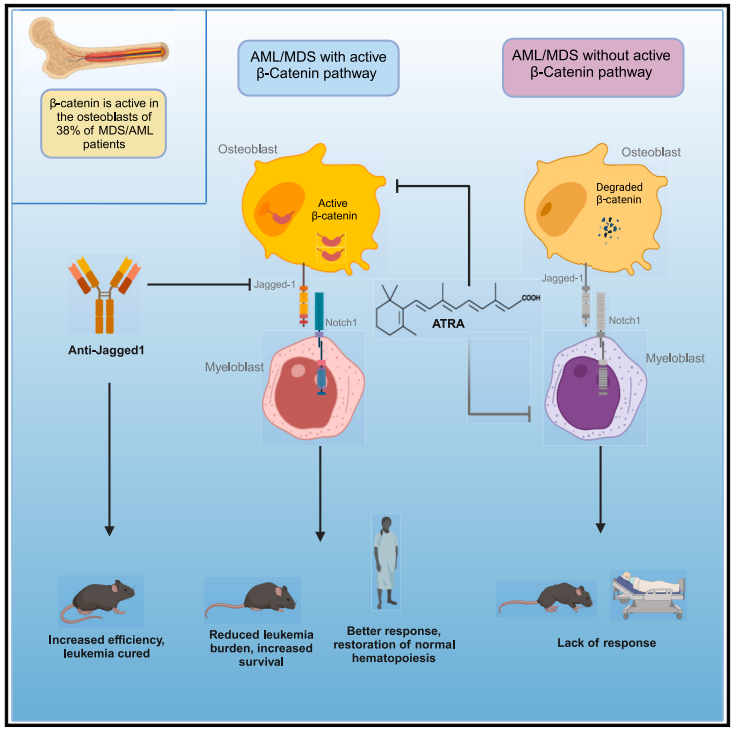

Highlights

- Activated β-catenin (βcat^{+}) in the stroma confers ATRA response in MDS/AML patients
- ATRA inhibits leukemic cell growth in MDS/AML patients with βcat^{+} osteoblasts
- Responsiveness is independent of cytogenetics, disease type, or mutational profile
- In mice, ATRA improves disease outcome without relapse

Authors

Ioanna Mosialou, Abdullah M. Ali, Rossella Labella, ..., Raul Rabadan, Azra Raza, Stavroula Kousteni

Correspondence

im2333@cumc.columbia.edu (I.M.), sk2836@cumc.columbia.edu (S.K.)

In brief

Mosialou et al. use malignant cells and osteoblasts from MDS/AML patients treated with ATRA in combination with hypomethylating agents or chemotherapy and β-catenin-induced AML mice to show that response to treatment depends on osteoblastic β-catenin activation. Responsiveness occurs independent of cytogenetics and mutational profile and shows no relapse in mice.

Mosialou et al., 2025, Cancer Cell *43*, 1–18
June 9, 2025
https://doi.org/10.1016/j.ccell.2025.03.007

CellPress

Please cite this article in press as: Mosialou et al., A niche driven mechanism determines response and a mutation-independent therapeutic approach for myeloid malignancies, Cancer Cell (2025), https://doi.org/10.1016/j.ccell.2025.03.007

Cancer Cell

CellPress

Article

A niche driven mechanism determines response and a mutation-independent therapeutic approach for myeloid malignancies

Ioanna Mosialou,[1,2,*] Abdullah M. Ali,[2,3,4,19] Rossella Labella,[1,19] Brygida Bisikirska,[1] Alvaro Cuesta-Dominguez,[1] Paraskevi Vgenopoulou,[1] Ismarc Reyes,[1] Sanjana M. Rao,[1] Anqi Wang,[5] Na Luo,[1] Marta Galan-Diez,[1,15] Junfei Zhao,[5,16] Brian J. Chernak,[6] Jan Philipp Bewersdorf,[7] Kazuya Fukasawa,[1,17] Jiayu Su,[5] Jason Higa,[8] Rachel A. Adams,[8] Adam L. Corper,[8] Sergey Pampou,[9] Catherine M. Woods,[8] Xiaomin Fan,[8] Roshan P. Shah,[10] Julie Feldstein,[7,18] Na Liu,[11] Cui Liang,[11] Maël Heiblig,[12] Steven Kornblau,[13] Guillermo Garcia-Manero,[13] Ellin Berman,[7] Joseph G. Jurcic,[6] Raul Rabadan,[2,5] Azra Raza,[2,3,4,6] and Stavroula Kousteni[1,2,3,14,20,*]

[1]Department of Physiology and Cellular Biophysics, College of Physicians and Surgeons, Columbia University Medical Center, New York, NY 10032, USA
[2]Edward P. Evans for Myelodysplastic Syndromes at Columbia University Medical Center, New York, NY 10032, USA
[3]Herbert Irving Comprehensive Cancer Center (HICCC), Columbia University, New York, NY 10032, USA
[4]Myelodysplastic Syndromes Center, Columbia University, New York, NY 10032, USA
[5]Program for Mathematical Genomics, Department of Systems Biology, Columbia University Medical Center, New York, NY 10032, USA
[6]Department of Med Hematology & Oncology, Columbia University Medical Center, New York, NY 10032, USA
[7]Department of Medicine, Memorial Sloan-Kettering Cancer Center, New York, NY 10065, USA
[8]AvantGen Inc, San Diego, CA 92121, USA
[9]Department of Systems Biology, Columbia University Medical Center, New York, NY 10032, USA
[10]Department of Orthopedic Surgery, Columbia University Medical Center, New York, NY 10032, USA
[11]Department of Hematology, Institute of Hematology, First Affiliated Hospital, Naval Medical University, Shanghai 200433, China
[12]Department of Hematology Centre Hospitalier Lyon Sud, 69495 Lyon, France
[13]Department of Leukemia, Division of Cancer Medicine, The University of Texas MD Anderson Cancer Center, Houston, TX 77030, USA
[14]Columbia Stem Cell Initiative, Columbia University, New York, NY 10032, USA
[15]Present address: Regeneron Pharmaceuticals, Inc, Tarrytown, NY 10591, USA
[16]Present address: Bristol Myers Squibb, Summit, NJ 07901, USA
[17]Present address: Department of Bioactive Molecules, Pharmacology, Gifu Pharmaceutical University, Gifu 501–1196, Japan
[18]Present address: Histowiz, Long Island 11101, USA
[19]These authors contributed equally
[20]Lead contact
*Correspondence: im2333@cumc.columbia.edu (I.M.), sk2836@cumc.columbia.edu (S.K.)
https://doi.org/10.1016/j.ccell.2025.03.007

SUMMARY

Myeloid cancers such as myelodysplastic syndromes (MDS) and acute myeloid leukemia (AML) remain resistant to standard of care (SOC) and targeted therapies. In this study, we demonstrate that responsiveness to therapy is associated with activation of β-catenin-JAG1 in osteoblastic cells of patients treated with all-*trans*-retinoic acid (ATRA). ATRA suppresses β-catenin activity in patients and leukemic mice. Consequently, it inhibits the growth and survival of MDS/AML cells from patients with active β-catenin-JAG1 signaling and promotes their differentiation. This occurs independently of cytogenetics and mutational profile. ATRA also improves disease outcome in mice with no evidence of relapse and a superior safety profile to SOC. A human anti-JAG1 antibody improves efficacy in leukemic mice and patient-derived MDS/AML cells. β-catenin activation provides an explanation for the differential response to ATRA and a mechanistic biomarker for ATRA repurposing in myeloid malignancies, potentially evading relapse and extending across a broad range of cancers.

INTRODUCTION

Myelodysplastic syndromes (MDS) and acute myeloid leukemia (AML) are aggressive hematological malignancies with a five-year overall survival as low as 5% for high risk MDS patients and 10–15% for elderly AML patients.[1–3] They are traditionally thought to arise from pre-malignant states via serial accumulation of mutations and epigenetic aberrations in hematopoietic stem and progenitor cells (HSPC).[4–10]

More recently, signals from the bone marrow (BM) stromal niche that alter the transcriptional milieu of hematopoietic stem cell (HSC) compartments have been shown to impact myeloid

Please cite this article in press as: Mosialou et al., A niche driven mechanism determines response and a mutation-independent therapeutic approach for myeloid malignancies, Cancer Cell (2025), https://doi.org/10.1016/j.ccell.2025.03.007

disease progression by promoting clonal expansion or transformation of normal or pre-leukemic HSCs leading to MDS and AML emergence.[11–17] Activation of β-catenin-Jagged-1 (Jag1) signaling in the osteoblastic lineage (osb-β-catenin) is a potent niche-driven tumorigenic signal present in approximately 40% of MDS and AML patients,[11] in del(5q)-associated myeloid malignancies[18,19] and following hypermethylation of its suppressors in patient stromal cells.[20] Its constitutive activation in mouse osteoblasts and progenitors induces MDS rapidly progressing to AML through osteoblastic upregulation of *Jag1* and subsequent induction of Notch1 signaling in HSCs.[11] These observations prompt to query whether targeting tumorigenic signals from stromal cells may provide a more genetically stable target overcoming mutation dependence and clonal resistance, thus, providing an efficient approach to manage disease and prevent relapse.

One such case of unexplained lack of treatment response is amply reported for all-*trans*-retinoic acid (ATRA),[21–35] the natural ligand of nuclear retinoid acid receptor (RAR). The success of ATRA therapy in acute promyelocytic leukemia (APL) spawned numerous attempts to translate this paradigm to AML/MDS. Clinical trials, few in MDS, the majority in AML, utilizing combination therapies with ATRA yielded disparate results.[21,22,36–41] Several large randomized trials failed to observe an advantage to adding ATRA to induction chemotherapy or low-dose cytarabine in AML patients[21–24,42] whereas others did.[25] Addition of ATRA to hypomethylating agents (HMAs)[42] showed that HMAs catalyze clinical activity of ATRA in relapsed/refractory (r/r) AML, a benefit not observed with low-dose cytarabine.[43] Transient responses were also observed with the RARα agonist tamibarotene in combination with 5-azacytidine (5-AZA) in patients with newly diagnosed AML.[44] However, in the trials with HMA combination, therapy response did not correlate with methylation status.[29] Thus, the mechanism(s) of response to treatment and these discrepant results are unknown.

In this study, we found that in addition to its ability to dissociate the NCOR-HDAC complex from RARα,[38,45–47] ATRA inhibits β-catenin functions. Therefore, we examined whether the basis of the differential response to ATRA may be activation of osb-β-catenin-Jag1 signaling in AML patients and whether inhibiting the oncogenic activity of osb-β-catenin-Jag1 has therapeutic potential in MDS and AML.

RESULTS

Activation of β-catenin in the osteoblastic lineage in 40% of MDS and AML patients is associated with worse survival

A cohort of 305 MDS and AML patients was screened for active nuclear osb-β-catenin (Figures S1A, S1B and Table S1) at diagnosis. The fraction of activated osb-β-catenin was significantly elevated in MDS (median: 8.0%), *De Novo* (median: 15.9%), and secondary AML transformed from MDS (sAML) (median: 23.7%) patients as compared to healthy individuals (median: 2.8%) (Figure 1A). Levels of osb-β-catenin activation did not correlate with β-catenin levels in $CD34^+$ cells (Figures S1C and S1D).

There were marked differences in disease severity, biology, and osb-β-catenin activation levels across MDS, AML, and sAML. To assess effects of active osb-β-catenin on overall survival (OS), such differences were normalized by defining cut-offs for β-cat^{high} patients (belonging to the top quartile) within each cohort. Active osb-β-catenin associated with worse OS in β-cat^{high} *De Novo* AML patients (Figure 1B) (median survival 12 months(mo) vs. 23months in β-cat^{low}) and in sAML patients (Figure 1C) (β-cat^{high}: 13months vs. β-cat^{low}: 18months), which was more pronounced in sAML, evident also in patients with median levels of active osb-β-catenin (β-cat^{med}: 10months vs. β-cat^{low}: 26months) (Figure 1D). A trend toward a worse OS in MDS patients was also observed (Figure S1E) (β-cat^{high}:112.1mo vs. β-cat^{low}:135mo). Re-stratification of patients in βcat^{low} or βcat^{high} using the same cut-off for all cohorts, defined by osb-β-catenin levels in all AML patients analyzed (Figures S1F–S1H) or the entire MDS/AML cohort (Figures S1I–S1L), led to similar results.

Furthermore, high levels of active osb-β-catenin were an independent risk factor for decreased OS in *De Novo* AML (hazard ratio [HR] 1.24, 95% confidence interval [CI] 0.98 to 1.57) and sAML (HR 1.46, 95% CI 0.94 to 2.27) (Table S1). This association remained following adjustment for confounders in multivariate Cox regression analysis (*De Novo* AML: HR 1.35, 95% CI 1.04 to 1.74; sAML: HR 1.36, 95% CI 0.84 to 2.20).

In summary, reduced survival and prevalence of osb-β-catenin activation were observed in at least 38% of MDS and AML patients, representing a significant patient subset carrying a common oncogenic molecular signature compared to other mutational signatures or past therapeutic target. This finding prompted us to examine whether inhibiting this pathway could improve disease outcome in this patient subset.

ATRA directly acts on osteoblasts to inhibit β-catenin nuclear activity

A search for Food and Drug Administration (FDA) approved compounds with β-catenin inhibiting properties identified ATRA as a candidate.[48,49] ATRA suppressed Wnt3a-induced nuclear localization of β-catenin and transcriptional activity in mouse and human primary osteoblasts (Figures 1E, S2A–S2D), including its downstream target, *Jag1*, shown to be required for leukemogenesis.[11] Expression and membrane protein levels of osb-β-catenin remained unaffected (Figures S2E and S2F) indicating that ATRA acts at a post-transcriptional level to suppress nuclear osb-β-catenin activity. Indeed, proteasomal inhibition abrogated the inhibitory effect of ATRA on β-catenin activity (Figures S2G and S2H) and increased ubiquitination of β-catenin was observed with ATRA (Figure S2I). Yet, ATRA inhibited a phosphorylation resistant constitutively active mutant form of β-catenin lacking exon3 (Figures S2J–S2L). Silencing the three known exon3/GSK3-independent ubiquitin ligases interacting with β-catenin C terminus, *Siah1*[50] and *Trim33*[51] or its armadillo repeat region, *c-Cbl*[52] (Figures S2M–S2O), did not abrogate ATRA action. ATRA upregulated the proteasomal pathway in primary human osteoblasts (Figure S2P), further suggesting an effect on proteasomal-mediated degradation. Expression of RARα transcriptional targets was also increased (Figure S2P) indicating a potential direct transcriptional effect of ATRA on genes encoding for proteasome 26S subunits.

ATRA responsiveness is correlated with activation of β-catenin-Notch signaling between osteoblasts and AML cells

We analyzed publicly available RNA sequencing (RNA-seq) data from $CD34^+$ cells isolated from patients that were treated with

Please cite this article in press as: Mosialou et al., A niche driven mechanism determines response and a mutation-independent therapeutic approach for myeloid malignancies, Cancer Cell (2025), https://doi.org/10.1016/j.ccell.2025.03.007

CellPress

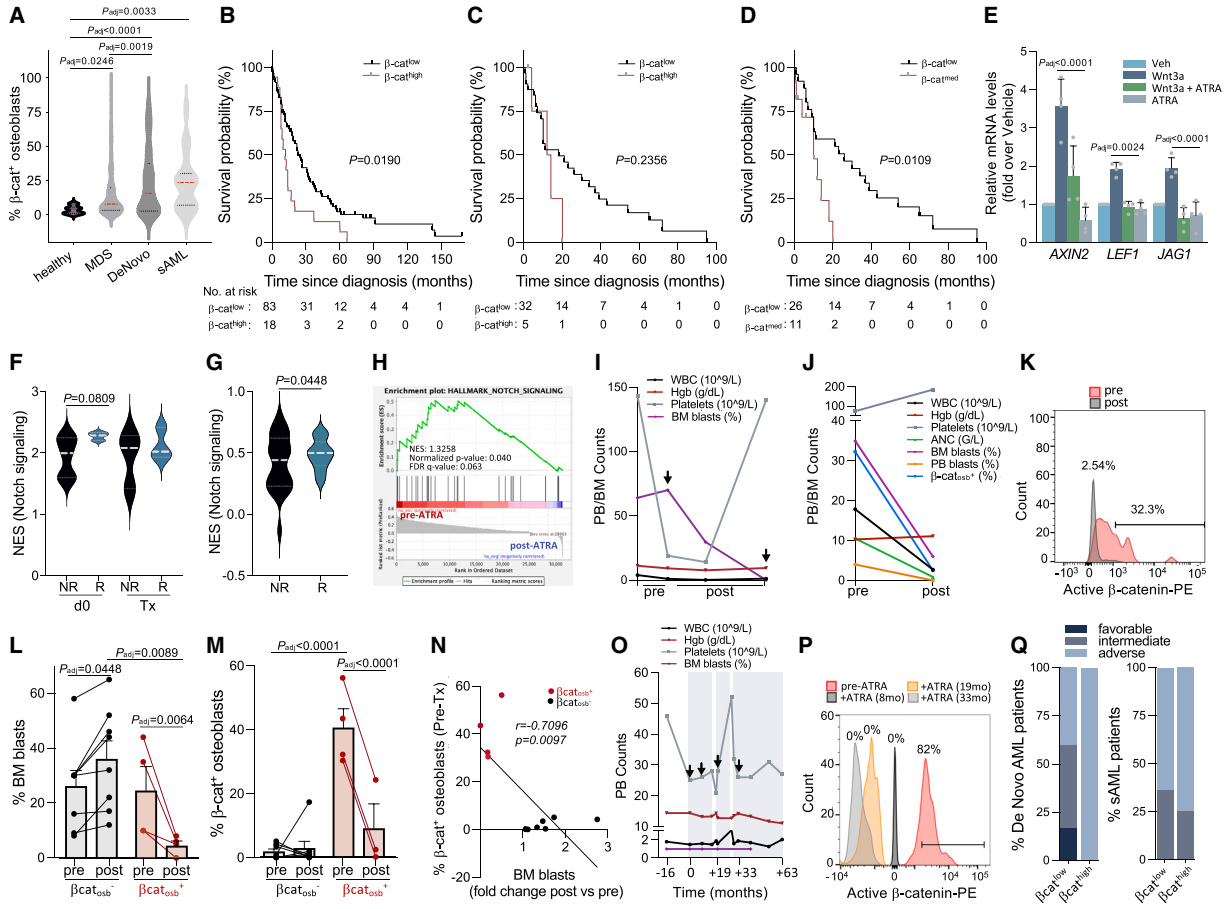

Figure 1. Osb-β-catenin activation associates with worse overall survival in AML patients and correlates with responsiveness to ATRA

(A) Osteoblasts (%) with nuclear active β-catenin from healthy (n = 21), newly diagnosed MDS (n = 183), *De Novo* (n = 100), or sAML (n = 22) patients.

(B–D) Kaplan-Meier survival curves of (B and C) βcat^{high} or (D) βcat^{med} (B) *De Novo* (n = 101) or (C and D) sAML (n = 37) patients, characterized at diagnosis by (B and C) the highest (top 25%) or (D) median levels of active osb-β-catenin, vs. βcat^{low}.

(E) Expression levels of β-catenin target genes, after normalization with *GAPDH* levels, in human primary osteoblasts treated with Wnt-3a and ATRA (n = 4).

(F and G) Notch transcriptional signature in CD34$^+$ cells from patients that responded (R) to ATRA+TCP versus non-responders (NR) (F) pre (d0) (NR, n = 5; R, n=3) and post-treatment (Tx) (n = 3) and (G) pretreatment from patients that were subsequently treated with ATRA+TCP or ATRA+VPA+theophyllamine (NR, n = 24; R, n = 12).

(H) Notch signaling and (I) peripheral blood (PB) counts (Hemoglobin (Hgb), white blood cell (WBC), platelets, absolute neutrophil counts (ANC)) and % BM blasts of an AML patient pre and post ATRA+FLAG+Thal chemotherapy. Arrows indicate time of sample collection for RNA-seq.

(J) Blood counts, % BM and PB blasts and % of osb-β-catenin of an AML patient pre and post ATRA+5-AZA+VPA.

(K) Flow cytometry plot of osb-β-catenin activity of the patient shown in (J).

(L) % BM blasts and (M) % active osb-β-catenin before and after ATRA treatment regimen in βcat$_{osb}^+$ (n = 4) or βcat$_{osb}^-$ (n = 8) AML patients pre-treatment.

(N) Pearson correlation analysis of % active osb-β-catenin in AML patients (n = 12) pre-treatment and change in BM blasts with treatment.

(O and P) (O) Blood counts and (P) % osb-β-catenin in an MDS patient pre- and post-ATRA monotherapy at the time points indicated. Arrows indicate time of sample collection. Gray shaded area indicates duration of ATRA treatment.

(Q) Distribution of βcat^{low} or βcat^{high} *De Novo* (left panel, βcat^{low}, n=42; βcat^{high}, n=10) or sAML (right panel, βcat^{low}, n=11; βcat^{high}, n=8) patients based on their ELN risk group.

In (A), (F), and (G) violin plots show data distribution. Lines represent median and quartiles. In (E), (L), and (M) data are presented as mean ± SEM. Statistical significance was calculated using (A) ordinary one-way ANOVA (Dunnett's multiple comparisons test), (B–D) Log rank (Mantel-Cox) test, (E, L, and M) two-way ANOVA or (F andG) two-sided, unpaired Student's t test. See also Figures S1–S3 and Tables S1–S3.

ATRA in combination with the lysine-specific histone demethylase 1A (LSD1) inhibitor tranylcypromine (TCP) in a phase I clinical trial (NCT02273102).[33] As a readout, we assessed activation of osb-β-catenin-induced Notch signaling in AML cells. Notch signaling was upregulated in CD34$^+$ cells from therapy responders compared to non-responders pre-treatment (Figure 1F). Moreover, treatment normalized Notch signaling levels. Combining these RNA-seq data with a second patient group treated with ATRA in combination with the histone deacetylase inhibitor (HDAC) valproic acid (VPA) and theophyllamine

Please cite this article in press as: Mosialou et al., A niche driven mechanism determines response and a mutation-independent therapeutic approach for myeloid malignancies, Cancer Cell (2025), https://doi.org/10.1016/j.ccell.2025.03.007

(NCT00175812)[34] showed consistent upregulation of Notch signature in responders compared to non-responders pre-treatment (Figure 1G). Validating this association, ATRA+FLAG+Thal chemotherapy regimen (Table S2) significantly decreased Notch signaling and BM-blasts in a refractory AML patient and stabilized declining platelet counts (Figures 1H and 1I). In contrast, ATRA+HAA chemotherapy (Table S2) had no effect and platelets continued to decline in an AML patient (Figure S3A) with unaltered Notch transcriptional signature and inactive osb-β-catenin (Figure S3B).

Analysis of BM biopsies from 12 other AML patients treated with ATRA in combination with the HMA 5-AZA alone or with the Bcl-2 inhibitor Venetoclax (VEN) or VPA (NCT00326170) (Figures 1J, 1K, S3C–S3M and Table S2) identified 4 patients in whom BM blasts were significantly decreased post-treatment and platelet counts increased or stabilized (Figures 1J, 1L, and S3C–S3E). Notably, all these patients showed high percentage of activated osb-β-catenin in pre-therapy samples but not during or post-treatment. In contrast, none of the patients with inactive osb-β-catenin pre-treatment (0/8) (Figures S3F–S3N), showed any improvement post-treatment. BM blasts increased and platelet counts continued declining. In all, there was a strong inverse correlation between baseline osb-β-catenin activity and BM blasts post-treatment ($r = -0.7096$, $p = 0.0097$) (Figures 1L-1N). Furthermore, although no BM biopsies were available at the time of best response (BR), an overall response rate of 100% was reached in patients with active baseline osb-β-catenin, as compared to 22% in patients without active osb-β-catenin, including 4 patients with complete response (CR) and 1 patient with CR without absolute neutrophil counts of more than 10^9/L (CRn) (Figure S3O and Table S2). Responsiveness was observed across patients with diverse cytogenetic and mutational profiles belonging to both intermediate and adverse risk groups.

Epigenetic effects of ATRA-induced NCOR-HDAC dissociation from RARα lead to reactivation of RARα transcriptional activity.[53] There was no difference in the expression of *RARα* and its transcriptional targets (*CDKN1A*, *TGM2*, *PRAM1*, and *DHRS3*) in hematopoietic cells from MDS (Figures S3P and S3Q) and AML patients (Figure S3R and Table S2) with (osb-β-catenin$^+$) and without (osb-β-catenin$^-$) activated osb-β-catenin or any association between levels of osb-β-catenin activation and *RARα* baseline expression levels (Figure S3Q). No difference in transcriptional signatures reflecting RARα activity was observed between CD34$^+$ cells from osb-β-catenin$^+$ and osb-β-catenin$^-$ patients (Table S2). Moreover, expression of *RARα* and its transcriptional targets did not differ at baseline between an osb-β-catenin$^+$ patient that responded to ATRA-containing regimen as compared to a non-responder osb-β-catenin$^-$ patient. Expression was rather decreased in the responder post-treatment (Figure S3R) suggesting that reactivation of RARα transcriptional activity is unlikely to be mediating response, at least in this patient.

This combined analysis of RNA-seq data and BM biopsies of 50 patient samples collected from four different study sites, demonstrated a strong association between inhibition of osb-β-catenin activity and/or Notch signaling in AML cells with ATRA, leading to AML improvement. Improvement occurred despite discontinuous dosing of ATRA and its diverse dosing schedule in combination with other therapeutic agents. Beneficial treatment response depended on and strongly associated with baseline osb-β-catenin activation (Fisher's exact test, $p = 0.021$, $n = 14$), whereas there was no association between response and the degree of global DNA hypomethylation or histone acetylation in combination treatments with 5-AZA/VPA.[29] Moreover, the single patient treated with ATRA in combination with 5-AZA/VEN (Figure S3C) relapsed while still on 5-AZA/VEN first-line treatment (Figure S3S) and CR was reached upon co-administration of ATRA, strengthening the role of ATRA in achieving the CR in this patient.

ATRA monotherapy of an MDS β-cat^{high} patient stabilized the worsening thrombocytopenia (Figure 1O). Disease improvement was marked by complete inhibition of osb-β-catenin activity (Figure 1P) and a parallel decrease in Notch signaling in the patient's MDS cells (Figure S3T). Expression of *RARα* and its transcriptional targets, except *CDKN1A*, was unaltered post-treatment (Figure S3T). During therapy, discontinuation of ATRA for short intervals due to toxicity (including xerostomia and intermittent skin rashes), decreased platelet numbers which reverted upon ATRA resumption (Figure 1O). The patient remained transfusion independent for at least 9 years, the entire follow-up duration.

These results suggest that responsiveness to ATRA (alone or in combination) is due to inhibition of activated osb-β-catenin, independent of RARα reactivation in hematopoietic cells and histone acetylation or DNA methylation changes due to VPA or 5-AZA combination, respectively.

βcat(ex3)$_{osb}$ leukemic mice represent a faithful model of βcat^{high} human AML

We sought to test the therapeutic efficacy of ATRA in osteoblast-triggered MDS/AML using a genetically engineered mouse model in which constitutive osb-β-catenin activation drives MDS progressing to AML (*βcat(ex3)$_{osb}$* mice).[11] Cytogenetic abnormalities and recurrent numerical and structural chromosomal aberrations present in myeloid cells of *βcat(ex3)$_{osb}$* mice.[11] Here, we identified AML relevant mutations in *Trp53*, *Gata2*, and *Cdkn2aip* (Table S3) in LSK(Lin$^-$c-Kit$^+$Sca1$^+$) cells from *βcat(ex3)$_{osb}$* mice and fusions of AML related genes, such as *Polr2j-Flt3*, *Cux1-Elf2*, and *Susd1-Cbfb* (Table S3). *Pml-Rarα* gene fusions, characteristic of APL, were not detected.

In agreement with genetic abnormalities in *βcat(ex3)$_{osb}$* mice, 25% of β-cat^{high} *De Novo* and 20% of β-cat^{high} sAML patients, while 10.4% and 8% of β-cat^{low}, respectively, showed complex karyotype (Table S1 and Figure S3U). Similarly, among complex karyotype *De Novo* and sAML patients, 37.5% belonged to osb-β-cat^{high}. Presence of del(7q) detected in *βcat(ex3)$_{osb}$* mice, and del(5q), shown to be associated with active osb-β-catenin signaling[18,19] were significantly enriched in β-cat^{high} *De Novo* and sAML patients (Table S1 and Figure S3U). Moreover, 100% of β-cat^{high} *De Novo* AML patients, for whom data were available, belonged to the adverse risk group compared to 40.5% of β-cat^{low} (Table S1 and Figure 1Q). An enrichment for adverse risk in sAML β-cat^{high} patients was also observed. Although data availability on patient mutational profile was limited, an enrichment for mutated *ASXL1*, *SRSF2*, *NRAS*, and *CBL* in β-cat^{high} *De Novo* AML patients was observed (Table S1). *TP53* mutations detected in *βcat(ex3)$_{osb}$* mice were significantly enriched among sAML β-cat^{high} patients, as were *IDH2* and *SRSF2* mutations (Table S1).

Please cite this article in press as: Mosialou et al., A niche driven mechanism determines response and a mutation-independent therapeutic approach for myeloid malignancies, Cancer Cell (2025), https://doi.org/10.1016/j.ccell.2025.03.007

CellPress

Comparison of the expression profile of CD34$^+$ cells isolated from AML βcat^{high} patients versus βcat^{low} with LSK cells from *βcat(ex3)$_{osb}$* mice versus their WT littermates, identified a distinct expression profile defined by β-catenin activation status (Figure S3V). A total of 146 gene signatures were commonly differentially expressed, with significant co-occurrence of positive or negative normalized enrichment scores (NES), in βcat^{high} AML patients and *βcat(ex3)$_{osb}$* mice (Figure S3W). Notably, characteristic of AML, those included upregulation of inflammatory cytokines production but downregulation of inflammatory response and immune response pathways and hallmark pathways of genomic instability (Table S3).

We considered whether common genetic aberrations in MDS/AML could lead to higher osb-β-catenin activation. However, mutations in *TP53*, *TET2*, and *FLT3^{ITD}* or *Nup98-HoxD13*, a common translocation in sAML, did not induce osb-β-catenin activation (Figures S3X and S3Y). Similarly, low (RCMD-RS) and high (RAEB2) risk MDS cells from osb-β-catenin$^+$ patients did not induce β-catenin activation following co-culture with primary human osteoblasts from healthy donors (Figure S3Z). Lack of osb-β-catenin activation was also observed following coculture of primary human osteoblasts from healthy subjects with the AML cell lines THP-1, U937, and Kasumi-1 (Figure S3Z), carrying mutations in *NRAS* and *TP53*; *PTEN*, *TP53*, *WT1*, and *PTPN11*; or *RAD21* and *TP53*, respectively. Thus, osb-β-catenin activation, at least in examined cases, is not an effect of MDS/AML. These data prompted us to use *βcat(ex3)$_{osb}$* mouse model, resembling the cohort of β-cat^{high} patients, to explore the therapeutic efficacy of ATRA in osb-β-catenin-driven MDS/AML.

ATRA improved disease outcome in *βcat(ex3)$_{osb}$* leukemic mice

ATRA was administered subcutaneously at 5 mg/kg 2x/week, 3–8x lower than the dose used on MDS/AML patients, to 10-day old *βcat(ex3)$_{osb}$* mice. All *βcat(ex3)$_{osb}$* mice are born with high risk MDS RAEBII phenotype[11] subsequently transforming to AML within the first week of life. ATRA abrogated constitutive active osb-β-catenin signaling in *βcat(ex3)$_{osb}$* mice as well as *Jag1* expression (Figures S4A and S4B).

Within a month post-treatment, the severe anemia and thrombocytopenia observed in *βcat(ex3)$_{osb}$* mice were reversed by ATRA (Figures 2A–2C and S4C–S4G) and effects persisted for 6 months. Disrupted spleen architecture was restored and BM-erythroid cells and megakaryocytes increased (Figure 2D). Leukocytopenia, lymphocytopenia and neutrophilia progressively normalized (Figures 2E–2G and S4H–S4J). ATRA reversed the increase in the long-term repopulating HSC progenitors (LT-HSC:LSKCD150^{high}CD48^{low}) (Figures 2H and S4K), the leukemia initiating population in *βcat(ex3)$_{osb}$* mice, and abolished myeloid block (Figures 2I and 2J) within a month which persisted for the duration the mice were observed (Figure 2H). Granulocyte monocyte progenitor (GMP; FcγRII/III$^+$/CD34$^+$) (Figures 2I and S4L) and immature myeloid progenitor (BM-IMP, c-Kit$^+$CD11b$^+$Gr1$^+$) numbers (Figure 2J) were restored while the percentage of the mature myeloid population (CD11b$^+$Gr1$^+$) remained elevated (Figures 2K and S4M) suggesting myeloid maturation with ATRA. Blasts were absent in blood and BM post-treatment (Figures 2L and 2M). As a result, survival was significantly prolonged (Figures 2N–2P). While all the vehicle-treated *βcat(ex3)$_{osb}$* mice died within a month, ATRA extended lifespan to at least 6 months in 60% of the *βcat(ex3)$_{osb}$* mice, the duration mice were monitored.

ATRA decreased Notch signaling in hematopoietic cells from *βcat(ex3)$_{osb}$* mice (Figures S4N and S4O), confirming that Jag1-Notch1 signaling is a main pathway downstream of activated osb-β-catenin mediating its leukemogenic effects. Corroborating our observations in patients, expression of *RARα,* its transcriptional targets (Figure S4O) and RARα signaling signatures (Table S3) was not different between LSK cells from *βcat(ex3)$_{osb}$* and WT littermates before or after ATRA treatment. Therefore, epigenetic effects of ATRA and NCOR/HDAC dissociation are unlikely since RARα is already active in hematopoietic cells. Lastly, ATRA improved AML without correcting the reported osteopetrosis of *βcat(ex3)$_{osb}$* mice,[54] nor changing circulating sclerostin levels (Figures S4P–S4R), indicating that its anti-AML effects are independent of effects on bone mass.

ATRA treated AML without inducing selection pressure and mutant clone outgrowth

Potential effects of ATRA treatment in the mutational profile were examined by whole-exome sequencing analysis of T and B cell depleted BM cells of *βcat(ex3)$_{osb}$* mice. Apart from a frameshift mutation (p.Ser64fs) in t*PHACTR4* in one of the mice unresponsive to ATRA (Table S3), commonly found in different tumors,[55] neither MDS/AML-relevant recurrent mutations nor copy-number variations (CNVs) (Figure S4S and Table S3) were identified in *βcat(ex3)$_{osb}$* mice, regardless of ATRA response. Therefore, ATRA treated AML in *βcat(ex3)$_{osb}$* mice without inducing selection pressure or mutant clone outgrowth.

Further examination indicated that an additional 4 mice (25%) died due to AML unrelated reasons (Figure S4T) with normal peripheral blood (PB) counts and absence of blasts (Figure S4U). Signs of gut toxicity (Figure S4V) were observed in two mice and hypercholesterolemia, and hypertriglyceridemia with hepatic lipid accumulation in the third (Figures S4U and S4V). Pancreatitis, a rare but serious adverse event encountered in ATRA-treated APL patients,[56–59] was a potential cause of death in the fourth, indicated by elevated serum amylase and lipase levels, and BM-CD4$^+$ cells (Figure S4U). Toxicities were not noted in the rest of the surviving *βcat(ex3)$_{osb}$* ATRA-treated mice, indicated by body weight gain (Figures 2N and 2O), normal liver and kidney function, and absence of inflammation (Figure S4W). T cell populations remained unaltered (Figures S4X and S4Y) while the reduced B cell lymphopoiesis of *βcat(ex3)$_{osb}$* mice was sustained (Figure S4Z). There were no changes in the hematological or blood chemistry profile of WT littermate controls post-ATRA treatment (Figures 2 and S4). Due to improvement in disease status, ATRA dosing was reduced to once/week from 2 months of treatment onwards.

ATRA specifically inhibited β-catenin-induced AML through its actions on osteoblasts

We examined whether the protective effect of ATRA occurs solely through inhibition of osb-β-catenin or whether hematopoietic cells were involved. *RARα* was the highest expressed subtype in mouse and human osteoblasts (Figures S5A and S5B) and its knockdown, but not *RARγ*, abrogated ATRA's inhibitory effect on β-catenin signaling (Figures S5C–S5F). Therefore, we

Please cite this article in press as: Mosialou et al., A niche driven mechanism determines response and a mutation-independent therapeutic approach for myeloid malignancies, Cancer Cell (2025), https://doi.org/10.1016/j.ccell.2025.03.007

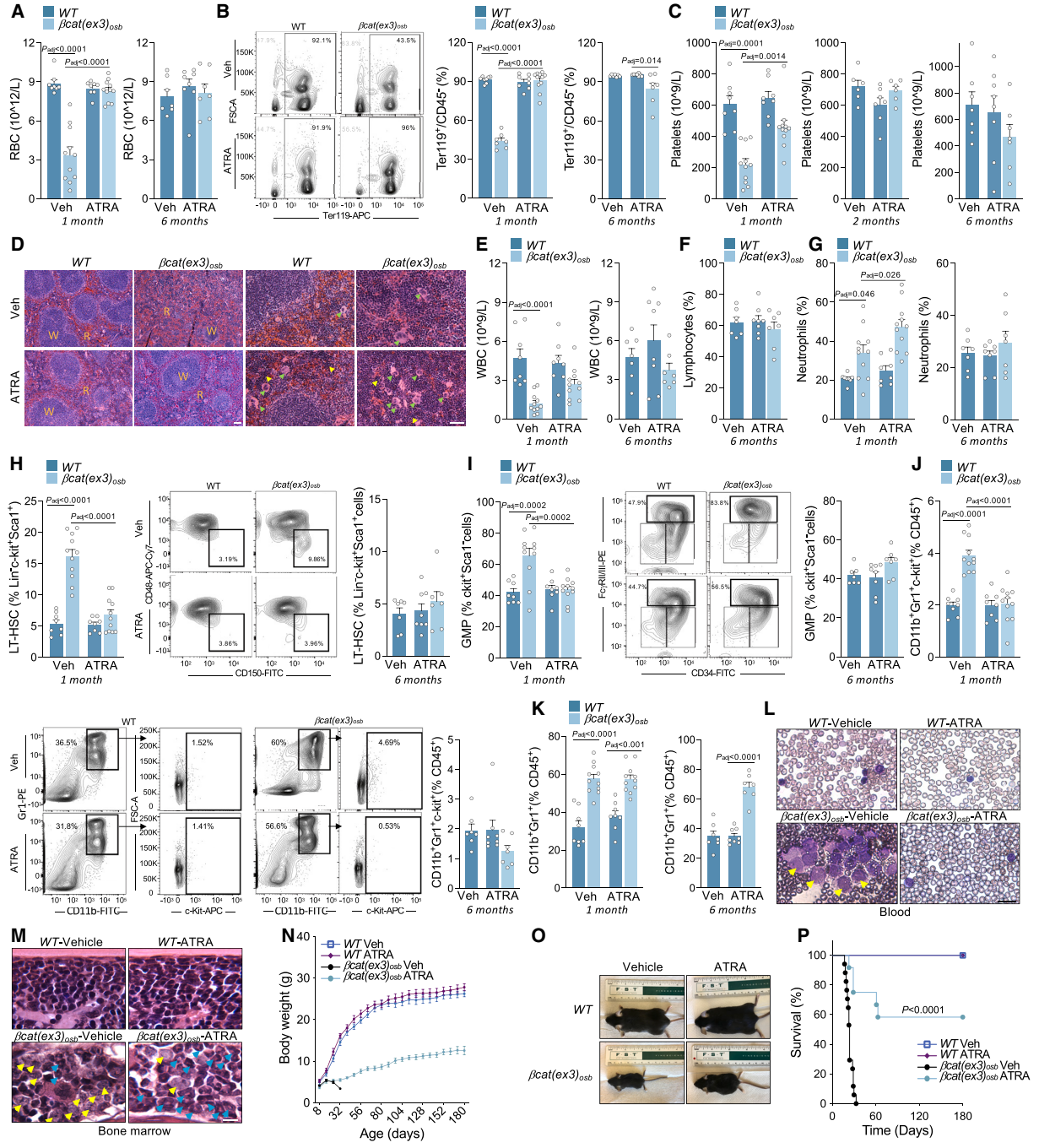

Figure 2. ATRA treatment improved disease outcome in *βcat(ex3)$_{osb}$* mice

(A–C) (A) PB red blood cell counts (RBC), (B) representative flow cytometry plots and quantification of BM erythroid progenitors, and (C) platelets in PB of WT and *βcat(ex3)$_{osb}$* mice following 1 (WT: n = 8/group; *βcat(ex3)$_{osb}$*: n = 11/group, except for *βcat(ex3)$_{osb}$* Veh in (B): n = 7), 2 (WT Veh: n = 6; WT ATRA: n = 7; *βcat(ex3)$_{osb}$* ATRA: n = 6) or 6 months (WT Veh: n = 7; WT ATRA: n = 8; *βcat(ex3)$_{osb}$* ATRA: n = 7) ATRA treatment.

(D) H&E staining of spleen sections from ATRA-treated WT and *βcat(ex3)$_{osb}$* mice. Yellow arrows: erythroid cells, green arrows: megakaryocytes, R: red pulp, W: white pulp. Scale bar: 100μm.

(E–K) (E) WBC, (F) lymphocytes and (G) neutrophils in PB and (H) LT-HSCs, (I) GMPs, (J) IMPs, and (K) mature myeloid cells in the BM of *βcat(ex3)$_{osb}$* mice and WT littermates following 1 (WT: n = 8/group; *βcat(ex3)$_{osb}$*: n = 11/group) or 6 months (WT Veh: n = 7; WT ATRA: n = 8; *βcat(ex3)$_{osb}$* ATRA: n = 7) ATRA treatment.

(legend continued on next page)

Please cite this article in press as: Mosialou et al., A niche driven mechanism determines response and a mutation-independent therapeutic approach for myeloid malignancies, Cancer Cell (2025), https://doi.org/10.1016/j.ccell.2025.03.007

CellPress

inactivated *RARα* in osteoblasts of *βcat(ex3)$_{osb}$* mice (*βcat(ex3)$_{osb}$;RARα$_{osb}^{-/-}$*) (Figures S5G–S5J) and treated them with ATRA as before.

ATRA inhibition of osb-β-catenin signaling was abrogated in *βcat(ex3)$_{osb}$;RARα$_{osb}^{-/-}$* mice (Figures S5K and S5L). Expression of *RARα* and its target genes was the same in LSK cells from *βcat(ex3)$_{osb}$;RARα$_{osb}^{-/-}$* and WT littermates (Figure S5M). Consequently, the protective effect of ATRA on disease development and progression was lost and *βcat(ex3)$_{osb}$;RARα$_{osb}^{-/-}$* mice succumbed to AML (Figures 3A–3N, S5N, and S5O). Thus, ATRA actions on osteoblasts are required for its protective effects in β-catenin-induced MDS and AML and are independent of hematopoietic reactivation of RARα. Reinforcing the specificity of ATRA therapeutic efficacy in osb-β-catenin-induced MDS/AML, osb-β-catenin activity and downstream signaling remained low pre- and post-ATRA in the mixed lineage leukemia MLL-AF9 protein fusion mouse model, (Figures S5P and S5Q). ATRA did not affect leukemia burden (Figures S5R–S5V), and OS was unchanged (Figure 3O;[60]). These findings provide a potential mechanistic explanation for the disparate results of ATRA treatment in AML patients.

Generation of a human monoclonal JAGGED1 blocking antibody

Similar to the mouse studies and the normalization of Notch signaling in ATRA responders, *JAG1* expression in patient osteoblasts highly correlated with activation levels of osb-β-catenin (Figure 4A). Thus, the entire pathway is conserved in MDS/AML patients and JAG1 can be an additional or alternative therapeutic target to inhibit downstream effects of osb-β-catenin.

To examine this hypothesis, we developed a human monoclonal antibody against JAG1 (anti-JAG1, D1). D1 binds to mouse (K_d = 0.091 nM) and human JAG1 (K_d = 0.074 nM) with high selectivity over other Notch1 ligands and potently inhibits JAG1-induced Notch1 signaling (IC50 = 40 pm) and transcriptional activity in OCI-AML3 cells co-cultured with *JAG1*-overexpressing osteoblasts (Figures S6A–S6E). D1 dose-dependently induced apoptosis (Figures 4B and S6F) and cell-cycle arrest (Figures 4C and S6G) of OCI-AML3 and THP-1 cells co-cultured with *JAG1*-overexpressing osteoblasts but not in monoculture confirming the growth-promoting effects of osb-JAG1 and a potential therapeutic benefit in blocking it.

Targeting JAGGED1 rescued *βcat(ex3)$_{osb}$* mice from AML

To test the antibody efficacy in human disease, we generated a human-mouse chimeric anti-JAG1 antibody that was equally potent to mouse D1 (Figures S6H and S6I). Single administration in WT mice at the dose sufficient to inhibit Notch-induced signaling in LSK cells of *βcat(ex3)$_{osb}$* mice, showed maximum blood concentration of 33.6 μg/mL in 24 h and a terminal half-life of 12 days (Figures S6J and S6K).

Weekly treatment with D1 (3 mg/kg, 1x/week), corrected all aspects of hematopoietic dysregulation in *βcat(ex3)$_{osb}$* mice (Figures 4D–4J and S6L–S6N), relieved myeloid block and promoted myeloid maturation, as myeloid cells were elevated (Figures 4K–4N). Blasts were eliminated from BM and blood (Figures 4O and 4P). In contrast to ATRA, D1 also improved B cell lymphocytopenia and T cell populations in the BM of *βcat(ex3)$_{osb}$* mice (Figures S6O and S6P). Body weight increased at a similar rate to that of WT littermates and lethality was abrogated (Figures 4Q and 4R). 10 of the 11 (91%) D1-treated mice survived for the 3 month-period of monitoring, while all mice treated with the isotype non-targeting IgG died within a month. Three D1-treated mice died of AML-independent reasons (one during phlebotomy, one with signs of gut toxicity and one due to unrelated infection) (Figure S6Q). No other overt side effects were noted in the rest of the mice and blood testing showed lack of liver or kidney toxicity or inflammation (Figure S6R). Confirming the specificity of action, D1 treatment had no effect on disease progression and OS of mice transplanted with MLL-AF9 cells (Figures 5A–5F).

Specific inhibition of β-catenin-JAG1 signaling was more effective and safer than SOC in MDS and AML

We compared the efficacy of blocking osb-β-catenin-JAG1 signaling with a SOC treatment regimen (five consecutive daily i.p. doses of cytarabine (100 mg/kg) along with doxorubicin for the first three days (3 mg/kg) [DA]) simulating induction chemotherapy in AML patients.[61] As expected, this regimen caused pancytopenia in WT mice (Figures 6A–6C), mimicking that of patients undergoing induction chemotherapy. However, in *βcat(ex3)$_{osb}$* mice, which already present with cytopenia, it exacerbated anemia, thrombocytopenia and leukocytopenia. Notably, SOC did not decrease blasts or the percentage of immature BM myeloid cells and led to higher lethality due to BM failure (Figures 6D–6G). Decreasing chemotherapy dose by half, although still able to induce a physiologically relevant response in WT mice (Figures 6H–6L), it failed to improve hematopoiesis and alleviate myeloid block in *βcat(ex3)$_{osb}$* mice (Figures 6J–6M). Expression of β-catenin transcriptional targets, including *Jag1*, was not affected by chemotherapy and remained elevated in *βcat(ex3)$_{osb}$* mice (Figure 6N). As a result, lethality was unaffected (Figures 6O–6Q).

Similarly, treatment with 5-AZA, 5 mg/kg/day i.p. for 5 days, equivalent to the human dose of 75 mg/m^2[62,63], caused cytopenia within 10-day treatment, from which WT mice recovered within 30 days (Figures 6R–6T). Blasts and immature cells accumulated in the BM (Figure 6U) and eventually survival of *βcat(ex3)$_{osb}$* mice was unchanged (Figures 6V and 6W). Expression of β-catenin transcriptional targets remained

(L and M) (L) Blood smears (Scale bar: 20μM) and (M) H&E staining of BM sections (Scale bar: 10μM) from ATRA-treated *βcat(ex3)$_{osb}$* mice and WT littermates. Yellow arrow, blasts; blue arrow, maturing myeloid cells.
(N–P) (N) Body weight (WT Veh: *n* = 7; WT ATRA: *n* = 10; *βcat(ex3)$_{osb}$* Veh: *n* = 13; *βcat(ex3)$_{osb}$* ATRA: *n* = 7), (O) representative images and (P) survival of WT and *βcat(ex3)$_{osb}$* mice following 6 months ATRA treatment (WT Veh: *n* = 7; WT ATRA: *n* = 10; *βcat(ex3)$_{osb}$* Veh: *n* = 16; *βcat(ex3)$_{osb}$* ATRA: *n* = 12).
Data are presented as mean ± SEM (A–C and E–K). Statistical significance was calculated using (A–C and E–K) ordinary one-way ANOVA or (P) log rank (Mantel-Cox) test. See also Figure S4 and Table S3.

Please cite this article in press as: Mosialou et al., A niche driven mechanism determines response and a mutation-independent therapeutic approach for myeloid malignancies, Cancer Cell (2025), https://doi.org/10.1016/j.ccell.2025.03.007

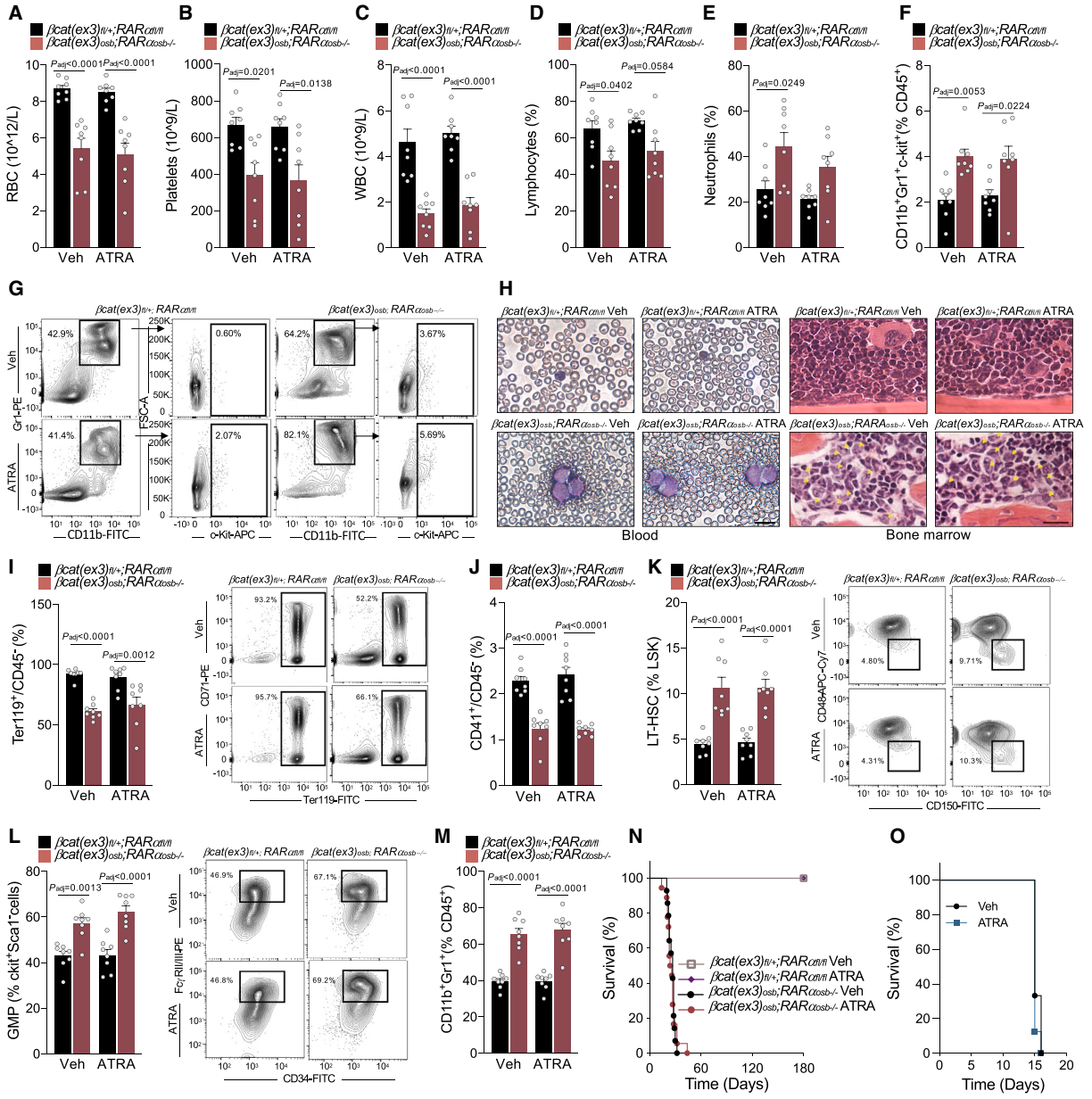

Figure 3. ATRA inhibited osb-β-catenin-driven AML by acting on osteoblasts

(A–M) (A) RBC, (B) Platelets, (C) WBC, (D) lymphocytes and (E) neutrophils in PB, (F) quantification of BM-IMP and (G) representative flow cytometry plots, (H) blood smears and H&E staining of BM sections (Scale bar: 20 μM; arrows: blasts), (I) erythroid progenitors, (J) megakaryocytes, (K) LT-HSCs, (L) GMPs and (M) myeloid cells in the BM of $\beta cat(ex3)_{osb};RARa_{osb-/-}$ mice and WT littermates following ATRA treatment (n = 8/group).

(N) Survival ($\beta cat(ex3)_{osb};RARa_{osb-/-}$ Veh: n=14; $\beta cat(ex3)_{osb};RARa_{osb-/-}$ ATRA: n = 18; WT: n = 7/group).

(O) Survival of WT mice injected with MLL/AF9-dsRed AML cells and treated with vehicle (n = 6) or ATRA (n = 8). Data are presented as mean ± SEM (A–F and I–M). Statistical significance was calculated using (A–F, I–M) ordinary one-way ANOVA or (N and O) log rank (Mantel-Cox) test.

See also Figure S5.

elevated (Figure 6X). These effects on $\beta cat(ex3)_{osb}$ mice are reminiscent of the effects seen during therapy in older patients with severe cytopenia or other medical comorbidities and more aggressive disease who cannot tolerate nor respond to aggressive standard treatments. Therefore, blocking osb-β-catenin-JAG1 signaling in osb-β-catenin-driven MDS/AML may be a more efficacious and safer therapeutic approach than SOC.

Please cite this article in press as: Mosialou et al., A niche driven mechanism determines response and a mutation-independent therapeutic approach for myeloid malignancies, Cancer Cell (2025), https://doi.org/10.1016/j.ccell.2025.03.007

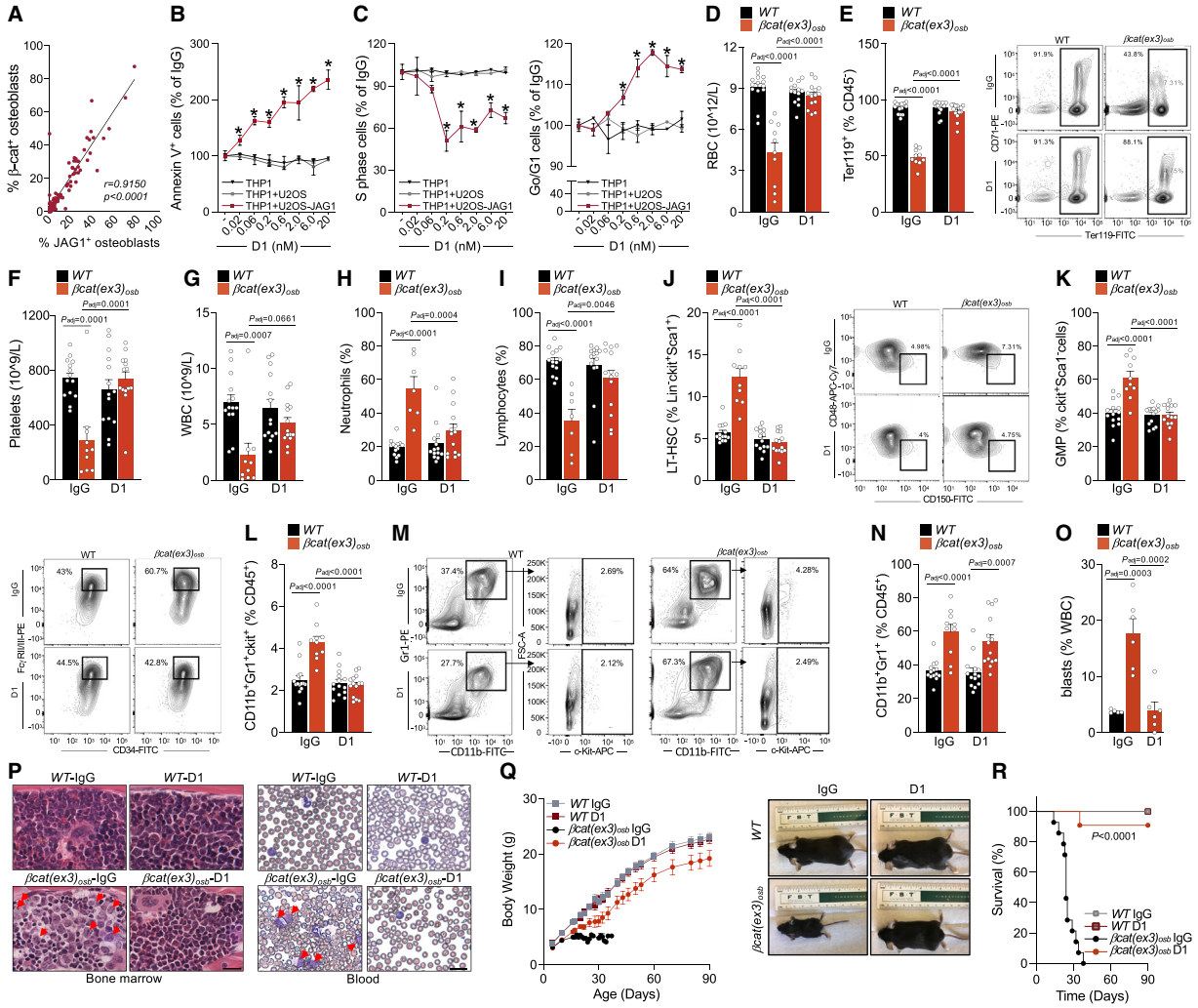

Figure 4. Targeting JAG1 rescued *βcat(ex3)$_{osb}$* mice from AML

(A) Pearson correlation analysis between JAG1 levels in MDS and AML patients' osteoblasts and activation levels of osb-β-catenin (n = 95).

(B–I) (B) % apoptotic and (C) proliferating (left) or quiescent (right) THP-1 cells treated with increasing concentrations of D1 or IgG for 24h in co-culture with U2OS cells (gray) or *JAG1*-overexpressing U2OS (red) or monocultured (black) (n = 2/group). Representative of 2 independent experiments. *p < 0.05 vs. IgG. (D) RBC, (E) BM-erythroid cells, (F) Platelets, (G) WBC, (H) neutrophils and (I) lymphocytes in PB.

(J–N) Representative flow cytometry plots and quantification of (J) LT-HSCs, (K) GMPs, (L and M) IMPs, and (M and N) myeloid cells in the BM of WT (n = 14/group) and *βcat(ex3)$_{osb}$* mice treated with D1 (n = 14) or IgG (n = 10) for 3 months.

(O) Blasts in PB (WT Veh: n = 5; *βcat(ex3)$_{osb}$* = 6/group).

(P) Blood smears and H&E staining of BM sections (scale bar: 20μM; arrows: representative blasts).

(Q and R) (Q) Body weight and representative mice images and (R) survival of WT (n = 14/group) and *βcat(ex3)$_{osb}$* mice treated with D1 (n = 11) or IgG (n = 14). Data are presented as mean ± SEM (B–L, N, O, and Q). Statistical significance was calculated using (B and C) two-way ANOVA, (D–L, N, and O) ordinary one-way ANOVA or (R) log rank (Mantel-Cox) test. See also Figure S6.

Inhibition of β-catenin-JAG1 in osteoblastic cells suppressed proliferation and survival and promoted differentiation of MDS and AML cells derived from patients across different disease categories

We sought to understand the range and specificity of a therapeutic approach inhibiting osb-β-catenin-JAG1 activation in patients. Lineage-depleted BM mononuclear cells (BMMNCs) isolated from osb-β-catenin$^+$ and osb-β-catenin$^-$ MDS and AML patients with distinct disease subtypes,[64,65] were co-cultured with BM mesenchymal stem cells (BM-MSCs) derived from the same patients (Table S4). Co-cultures were treated with ATRA or D1.

Each treatment significantly reduced actively proliferating cells specifically from osb-β-catenin$^+$ MDS/AML patients compared to vehicle treatment (Figure 7A). ATRA led to a 50% decrease, while D1 led to a reduction of up to 70% in MDS patient-derived cells. Simultaneously, ATRA or D1 decreased survival of cells from

Please cite this article in press as: Mosialou et al., A niche driven mechanism determines response and a mutation-independent therapeutic approach for myeloid malignancies, Cancer Cell (2025), https://doi.org/10.1016/j.ccell.2025.03.007

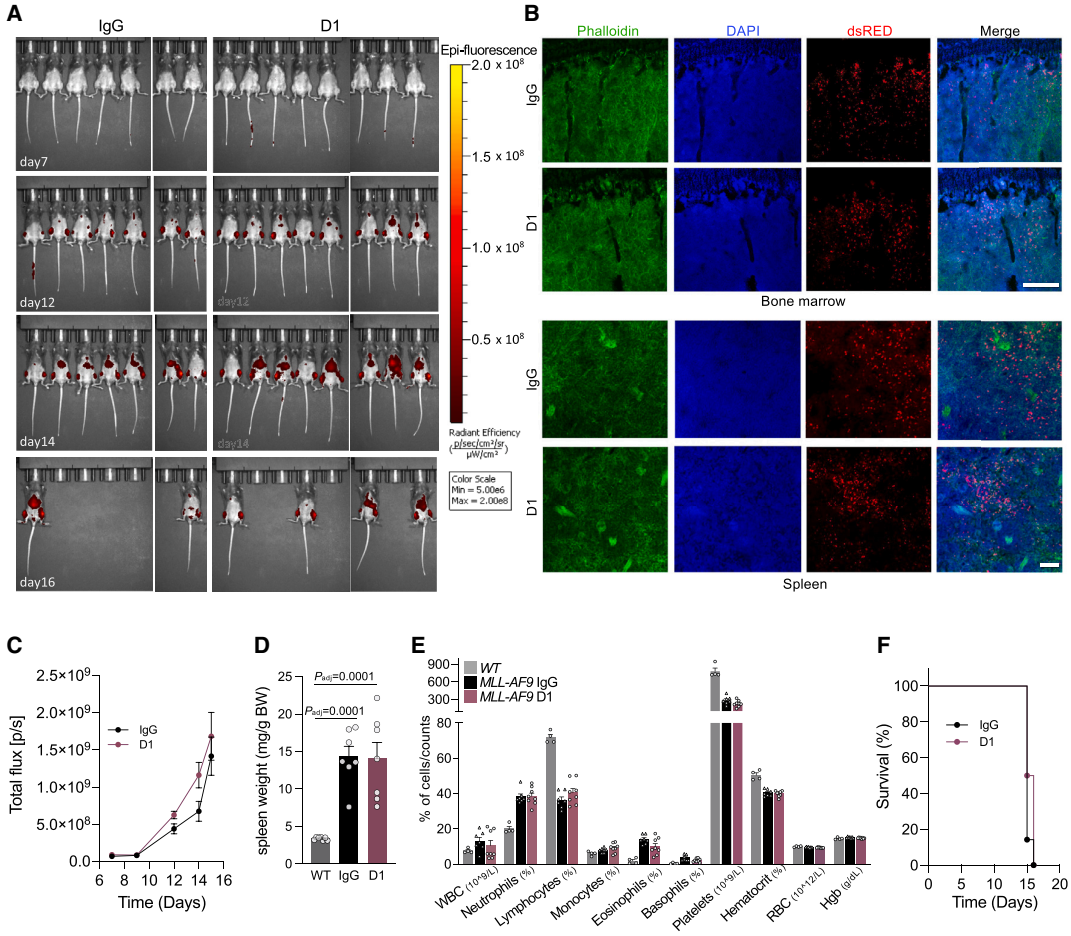

Figure 5. Targeting JAG1 specifically inhibited osb-β-catenin/JAG1-driven AML

(A and C) (A) Representative images and (C) quantification of leukemia progression determined by dsRed fluorescence at the indicated days of WT mice injected with MLL/AF9-dsRed AML cells and treated with D1 (n = 8) or IgG (n = 7).

(B, D, and E) Representative images of MLL/AF9-engrafted tissues (scale bar: BM 100 μM, spleen 50 μM), (D) spleen weight, (E) complete blood counts and (F) survival of the same mice (D1: n = 8; IgG: n = 7). In (D and E), the same WT un-injected controls (n = 4), used in Figures S5U and S5V are included for comparison.

Data are presented as mean ± SEM (C–E). Statistical significance was calculated using (D and E) ordinary one-way ANOVA or (F) log rank (Mantel-Cox) test.

osb-β-catenin$^+$ MDS and AML patients by 100% and 40% respectively; overall, there was no effect in cells from osb-β-catenin$^-$ patients or from healthy subjects (Figure 7B). The magnitude of the response to either treatment correlated with the levels of osb-β-catenin-JAG1 activation underlining the specificity of ATRA and D1 action (Figures 7C and 7D). Moreover, ATRA/D1 combination did not significantly improve the effects of each treatment alone (Figures S7A and S7B), suggesting they both act on the same pathway to suppress cell proliferation and survival in osb-β-catenin$^+$ patients. There was no difference in MDS/AML cell proliferation and survival pre-treatment among osb-β-catenin$^+$ and osb-β-catenin$^+$ patients (Figures S7C and S7D).

Cells from all osb-β-catenin$^+$ MDS patients responded to the cytostatic properties of D1, and 56% of them responded to ATRA (Figures 7A, 7E, and 7F). Additionally, 62.5% and 75% of them responded to the cytotoxic properties of D1 and ATRA, respectively (Figures 7B, 7E, and 7F). Among AML patients, cells derived from approximately 85% of those patients showed decreased proliferation upon ATRA and D1 (Figures 7A and 7G–7I) while 85% and 59% showed decreased viability upon ATRA and D1, respectively (Figures 7B and 7G–7I). Responsiveness was observed across patients with diverse mutational profiles (Figure 7J), disease types and categories, and cytogenetics (Figures 7E–7I). The only factor that was significantly associated and could predict response was activation of osb-β-catenin (Figure 7K).

Similarly, D1 and ATRA promoted myeloid and erythroid differentiation specifically in AML cells from osb-β-catenin$^+$ patients, indicated by increased numbers of CD11b$^+$ and CD15$^+$ cells (Figures 7L–7N) or Band 3$^+$ and glycophorin A$^+$ (Figures 7O–7Q), respectively. Response was associated with activation of osb-β-catenin and no effects were observed in cells from

Please cite this article in press as: Mosialou et al., A niche driven mechanism determines response and a mutation-independent therapeutic approach for myeloid malignancies, Cancer Cell (2025), https://doi.org/10.1016/j.ccell.2025.03.007

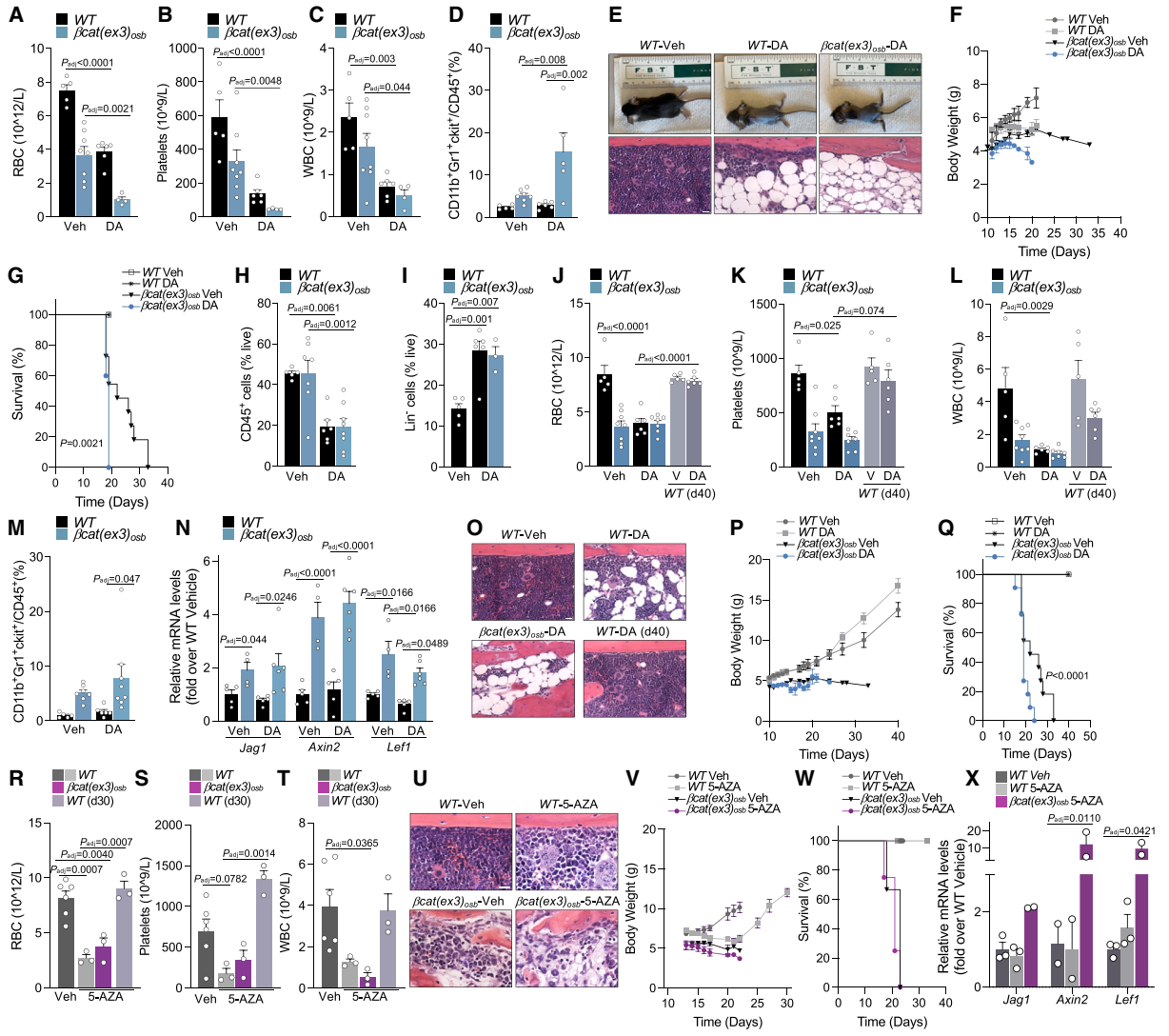

Figure 6. Chemotherapy increased lethality without curing leukemia in *βcat(ex3)$_{osb}$* mice

(A, J, and R) RBC, (B, K, and S) platelets, (C, L, and T) WBC, (D and M) BM-IMPs, (E, O, and U) representative images of H&E stained BM sections (Scale bar: 20μM), (F, P, and V) body weight, (G, Q, and W) survival, (H) % BM-CD45$^+$ cells, (I) % BM-Lin$^-$ cells and (N and X) expression of β-catenin target genes, after normalization with *Actb* levels, in BM-free bones of *βcat(ex3)$_{osb}$* mice and WT littermates treated with (A–G) DA or (H–Q) half-dose DA or (R–X) 5-AZA. WT Veh: n = 5 (In R–T, V, and W: n=6, X: n=3); WT DA: n = 6 (in N, n = 5); WT 5-AZA: n=3; *βcat(ex3)$_{osb}$* Veh: n = 8 (A–C, J–L), 7 (D, H, and M), 4 (N), 11 (F, G, P, and Q), 3 (V and W). *βcat(ex3)$_{osb}$* DA: n = 4 (A–C), 5 (D, F, and G), 8 (H and M), 6 (N), 3 (I), 7 (J–L), 11 (P and Q); *βcat(ex3)$_{osb}$* 5-AZA: n=3 (R–T), 4 (V and X), 2 (X). For comparison, the same group of vehicle-treated *βcat(ex3)$_{osb}$* mice are included in panels A–G and J–Q.

Data are presented as mean ± SEM (A–D, F, H–N, P, R–T, V, and X). Statistical significance was calculated using (A–D, H–M, R–T) ordinary one-way ANOVA, (N and X) two-way ANOVA or (G, Q, and W) log rank (Mantel-Cox) test.

osb-β-catenin$^-$ patients. The magnitude of myeloid and erythroid induction positively correlated with levels of osb-β-catenin-JAG1 activation (Figures 7R–7U).

Identification of a circulating skeletal stem cell population that expresses activated β-catenin allows for patient stratification

To streamline selection of candidates for ATRA or anti-JAG1 therapy and monitor response post-treatment we searched for a surrogate of osb-β-catenin activation in PB. *Runx2* is expressed in plasmacytoid dendritic cells and downregulates chemokine receptor *Cxcr4* expression, allowing for BM egress.[66] *Runx2* is expressed in uncommitted osteoprogenitors[67] and *Cxcr4* is expressed in skeletal stem cells.[68,69] Thus, we examined whether a skeletal stem population could be egressing and be detectable in PB. Flow cytometry of PB mononuclear cells (PBMCs) from MDS and AML patients identified a unique population of circulating cells that are not hematopoietic

Please cite this article in press as: Mosialou et al., A niche driven mechanism determines response and a mutation-independent therapeutic approach for myeloid malignancies, Cancer Cell (2025), https://doi.org/10.1016/j.ccell.2025.03.007

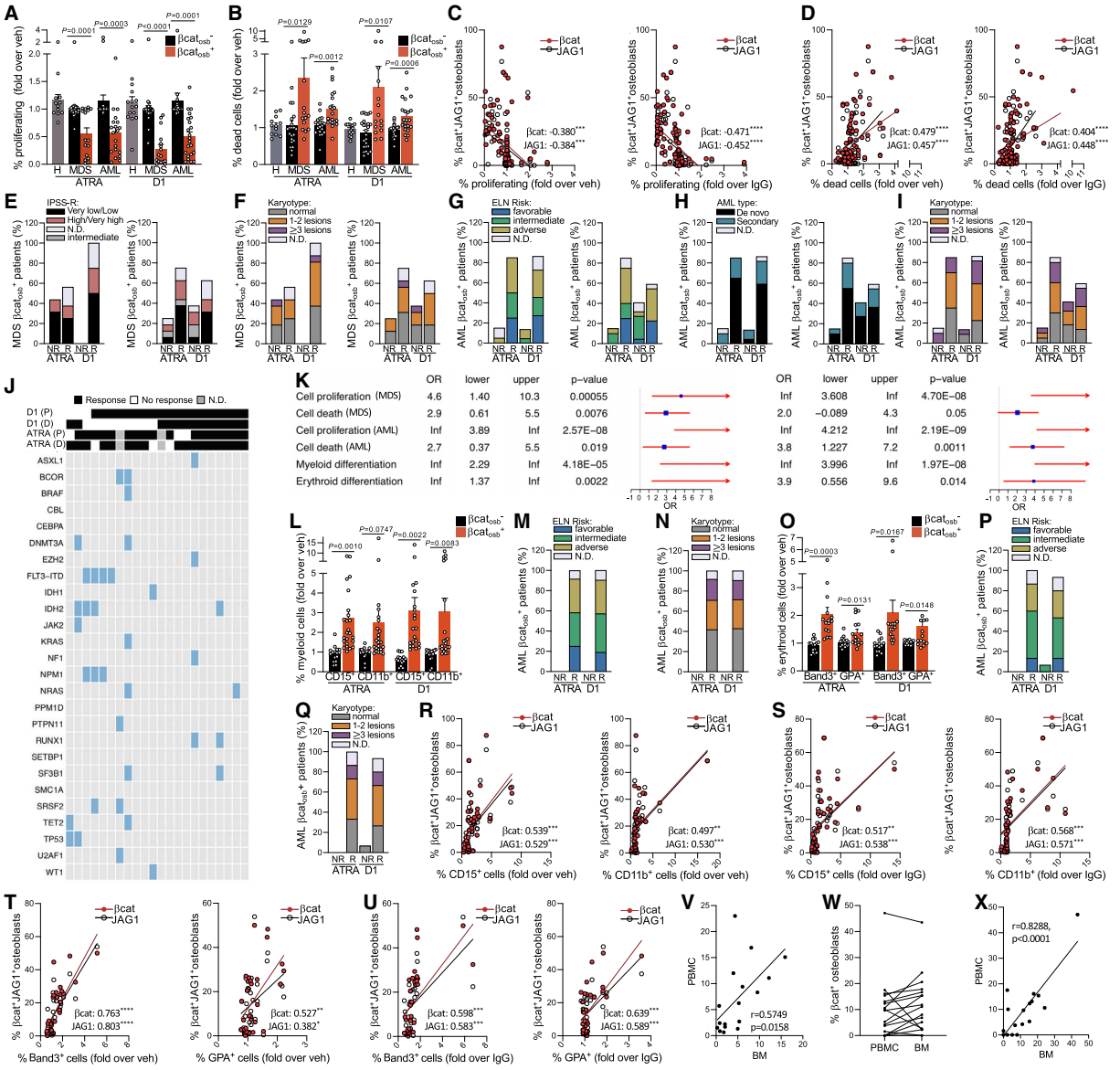

Figure 7. ATRA and D1 suppressed proliferation and survival and promoted differentiation of MDS/AML cells from βcat$_{osb}^+$ patients

(A–D) (A) % Edu$^+$, (B) % dead cells, and (C–D) Pearson correlation analysis of % βcat$^+$JAG1$^+$ osteoblasts with % of (C) Edu$^+$ and (D) dead cells from βcat$_{osb}^+$ or βcat$_{osb}^-$ MDS (βcat$_{osb}^+$, n = 16/group; βcat$_{osb}^-$ ATRA, n = 22; βcat$_{osb}^-$ D1, n = 25) or AML (ATRA, n = 20/group; D1, n = 22/group) patients or healthy (H) subjects (ATRA, n = 12; D1, n = 15) following ATRA (C and D left panel) or D1 (C and D right panel) treatment for 24h in co-culture with their BM-MSCs. $^{***}p \leq 0.001$, $^{****}p \leq 0.0001$.

(E–I) % of βcat$_{osb}^+$ (E and F) MDS and (G–I) AML patients from different (E) IPSS-R or (G) ELN risk groups, (H) disease types or (F and I) cytogenetic groups that responded (R) or not (NR) to the cytostatic (left) or cytotoxic (right) properties of ATRA or D1 (E and F: n = 16/group; G–I: ATRA, n = 20; D1, n = 22).

(J) Mutational status of R versus NR to ATRA (n = 20) and D1 (n = 22) among βcat$_{osb}^+$ AML patients. (P: proliferation, D: cell death).

(K) Forestplot of β-catenin activation status in osteoblasts and response to ATRA (left) or D1 (right) for the parameters indicated. Log2 Odds ratio (OR) values and their 95% CI are shown.

(L–Q) (L) % CD11b$^+$ or CD15$^+$ cells, (M and N) % of βcat$_{osb}^+$ R vs. NR AML patients based on ELN risk (M) or cytogenetics (N), (O) % Band3$^+$ or GPA$^+$ cells, (P and Q) % of βcat$_{osb}^+$ R vs. NR AML patients based on ELN risk (P) or cytogenetics (Q).

(R–U) Pearson correlation analysis of βcat$^+$JAG1$^+$ osteoblasts (%) with (R and S) % of CD15$^+$ (left) or CD11b$^+$ (right) cells, and (T and U) % of Band3$^+$ (left) or GPA$^+$ (right) cells following co-culture for 7 days under (L–N, R and S) myeloid (βcat$_{osb}^+$ ATRA, n = 24; D1, n = 2; βcat$_{osb}^-$, n = 16/group) or (O–Q, T, and U) erythroid

(legend continued on next page)

Please cite this article in press as: Mosialou et al., A niche driven mechanism determines response and a mutation-independent therapeutic approach for myeloid malignancies, Cancer Cell (2025), https://doi.org/10.1016/j.ccell.2025.03.007

(Lin$^-$CD34$^-$), but express *Runx2* and notably, osteocalcin (OCN). This population comprised ~5% of total PBMCs post-exclusion of hematopoietic lineage cells and its numbers in individual subjects tightly correlated with the fraction of marrow osteoblastic lineage cells (r = 0.5749, p = 0.0158) (Figure 7V). More importantly, activation of β-catenin in these circulating skeletal stem cells (cSSCs)[70] highly and significantly correlated (r = 0.8288, $p < 0.0001$) with the levels of β-catenin activity in BM osteoprogenitors (Figures 7W, 7X, and S7E). Therefore, circulating Lin$^-$CD34$^-$Runx2$^+$OCN$^+$ cells are a surrogate cSSC population reflecting osb-β-catenin activation and can serve as a biomarker to predict response to ATRA and anti-JAG1 treatment, allowing for rapid and non-invasive patient selection and disease follow-up.

DISCUSSION

We demonstrate a mechanism of ATRA action comprising of inhibition of activated osb-β-catenin-JAG1 signaling. Our observations suggest that the basis of disparate effects across ATRA-treated AML patients may result from a common underlying alteration in the responding patient population: activation of osb-β-catenin-JAG1 signaling.

There was a lack of consistent response to ATRA in combination with low-dose cytarabine, etoposide, hydroxyurea, and others.[42,43] An anti-leukemic effect has been reported in MDS and AML patients upon addition of ATRA to HMAs, such as decitabine[28,71] or 5-AZA in combination with VPA.[29] Similarly, the DECIDER study showed significant improvements with ATRA addition to decitabine, in both objective response rate and OS,[31] yet extended survival in the decitabine/ATRA arm was not fully explained by improvements in response rates, suggesting that another mechanism should explain the prolonged disease-stabilizing effect of ATRA therapy. When we examined BM biopsy samples from patients in NCT00326170 trial, in which response was not associated with DNA methylation and histone acetylation,[29] we found that treatment response was associated instead with baseline activation of osb-β-catenin, which was suppressed post-treatment. Notably, development of secondary resistance to 5-AZA/VEN in an AML patient was associated with activation of osb-β-catenin. Subsequent ATRA co-administration suppressed osb-β-catenin activation and achieved CR in this patient. More recently, a similar triplet therapy (ATRA+5-AZA/VEN) achieved a high CR rate in newly diagnosed AML (NCT05654194).[72] There is a lack of studies of ATRA as a monotherapy. Additionally, ATRA effects on the stroma may have been poorly reflected as a 3- to 8-fold higher dose was employed in the trials than the one used in our mouse studies. This led to higher toxicity and a shorter duration of therapy. A lower dose, longer-term therapy may be necessary to achieve the effects we have observed in murine models. Moreover, the lack of biomarker for responders may have hidden the response of some patients in these studies. As we characterize the overall percentage of advanced osb-β-catenin$^+$ MDS/AML patients, it may be that the clinical trials done had a selection bias that obscured possible responses.

Hypermethylation of the upstream negative regulator of β-catenin, Frizzled Related Protein (FZDB), is involved in the activation of osb-β-catenin signaling in MDS patients.[20] Thus, the preferential beneficial synergistic effect observed in prior studies in combination with HMAs,[27,29,31,71] as compared to chemotherapy,[41–43] could in part be due to the simultaneous targeting of activated β-catenin at two levels, by directly or indirectly inhibiting its induction with HMAs and directly inhibiting β-catenin nuclear activity with ATRA. Taken together, these observations support ATRA's specific abrogation of osb-β-catenin signaling as at least an important contributor for the observed anti-leukemic benefit in clinical trials with HMA combination.

A higher objective response rate to ATRA-HMA combination was also reported in patients with *TP53* mutations.[73] This could be important since β-cat^{high} patients also present with complex karyotype, del(5q) and del(7q), often co-occurring with *TP53* inactivating mutations.[74–82] Additionally, in our study, among *TP53*-mutant patients, 33.3% of them had active osb-β-catenin. A potential association between active osb-β-catenin and *TP53* inactivating mutations and complex karyotype, needs to be investigated in future studies.

Moreover, targeting specifically the downstream JAG1 signaling pathway, rather than Notch, with anti-JAG1 antibody hindered AML progression, cured leukemia and re-established trilineage hematopoiesis in mice. Notably, this treatment overcame resistance observed in 40% of ATRA-treated mice without any obvious toxicity. ATRA toxicity has been reported in patients,[56–59,83–85] which was also noted in 25% of ATRA-treated mice. In light of the 91% efficacy of anti-JAG1 in curing leukemia in mice and lack of toxicity encountered, its development may be a more efficient and safe therapeutic approach.

These observations advance our understanding of niche-derived signals, substantiating their involvement in disease pathogenesis. Moreover, they provide a mechanistic explanation for the lack of consistent response to ATRA that could significantly impact treatment of the approximately 40% of MDS and AML patients that have activated osb-β-catenin-JAG1 signaling, a significantly large genetically defined group among WHO subtypes. Lastly, inhibition of β-catenin activity by ATRA did not require exon3, the most affected region driving constitutive activation of β-catenin. Therefore, ATRA may find application in the treatment of additional cancer types caused by dysregulation in the APC/GSK3β-axis, such as hepatocellular carcinoma,[86] colorectal,[87] and breast[88] cancer and as an adjunctive therapy in pancreatic cancer.[89]

(n = 15/group) differentiation conditions with BM-MSCs and treated with (L–R, and T) ATRA or (L–Q, S, and U) D1. *$p \leq 0.05$, **$p \leq 0.01$, ***$p \leq 0.001$, ****$p \leq 0.0001$.

(V) Pearson correlation analysis of the fraction of Lin$^-$CD34$^-$Runx2$^+$OCN$^+$ cells in PBMCs of MDS and AML patients with the same cell population in their BM (n = 17).

(W and X) (W) % Lin$^-$CD34$^-$Runx2$^+$OCN$^+$ cells with active β-catenin and (X) Pearson correlation analysis of β-catenin activation status in PBMCs and BM cells of the same patients (n = 17). Data are presented as mean ± SEM (A, B, L, and O). Statistical significance was calculated using (A, B, L, and O) two-sided, unpaired Student's t test or (K) Fisher's exact test. See also Figure S7 and Table S4.

Please cite this article in press as: Mosialou et al., A niche driven mechanism determines response and a mutation-independent therapeutic approach for myeloid malignancies, Cancer Cell (2025), https://doi.org/10.1016/j.ccell.2025.03.007

Limitations of the study

This study shows that activation of osb-β-catenin mediates ATRA responsiveness in MDS and AML patients. Further investigation and extensive validation in a larger cohort of patients is required to unequivocally establish osb-β-catenin as a biomarker prior to its implementation in clinical practice. Clinical biomarker validation is a complex process and comprehensive assessment of its suitability requires a clinical trial that is beyond the scope of this manuscript. It is possible that the therapeutic effects of ATRA observed in our mouse model might be partly because osb-β-catenin overactivation is the leading cause of AML in this model, and this might not be equally important in other AMLs where osb-β-catenin activation is a contributing but not leading factor. Such a possibility will be tested in future studies using additional AML and patient-derived xenongraft (PDX) mouse models. Lastly, additional studies are needed to mechanistically dissect the exact molecular mechanisms involved in ATRA induced degradation of osb-β-catenin.

RESOURCE AVAILABILITY

Lead contact

Requests for further information and resources should be directed to and will be fulfilled by the lead contact, Stavroula Kousteni (sk2836@cumc.columbia.edu).

Materials availability

There are restrictions to the availability of anti-JAG1 antibody since it was generated by a commercial entity (AvantGen Inc).

Data and code availability

Exome sequencing data for ATRA-treated mice were deposited at NCBI SRA (BioProject accession number PRJNA967739) and is publicly available. Original Western blot images from Figures S2B, S2E, S2H, S2I, and S2L were deposited at Mendeley (https://data.mendeley.com/datasets/75jjmbkft7/1) and are publicly available. RNA-seq data from ATRA-treated patients, $CD34^+$ cells from βcat^{high} and βcat^{low} AML patients, LSK cells from $\beta cat(ex3)_{osb}$ mice and their WT littermates and primary human osteoblasts from healthy donors treated with Wnt3a+ATRA were deposited at Gene Expression Omnibus under accession code GSE262907, GSE277103, GSE277597, and GSE277588, respectively, and are publicly available. Gene expression matrices from ATRA clinical trials are publicly available and were downloaded from Gene Expression Omnibus under accession code GSE151594[33] and GSE106096.[90] This paper does not report original code. Any additional information required to reanalyze data reported in this paper is available from the lead contact.

ACKNOWLEDGMENTS

We thank Martin Caroll, M.D. and Riccardo Dalla Favera, M.D. for discussions and critical reading of the manuscript; Martin Caroll, M.D. for providing patient samples; Matthews Jairo and Mumtaz Muhammad for help with patient-derived biopsies, Pierre Chambon, M.D. for providing the $RAR\alpha_{fl/fl}$ mice; Aaron Viny, M.D. for providing the $Flt3_{fifl}$ mice, Gerard Karsenty, M.D., Ph.D. for providing β-catenin expression vectors, and the Columbia University's Institute of Comparative Medicine Diagnostic Laboratory for blood chemistry analyses. These studies used the shared resources of Columbia Genomics and High Throughput Screening Shared Resource (funded in part through the NIH/NCI Cancer Center Support Grant P30CA013696), the Molecular Pathology Shared Resource (MPSR), the Cancer Center Flow Core facility (funded in part through Center Grant P30CA013696), the CSCI Flow core facility and the Oncology Precision therapeutics and Imaging Core (OPTIC) at the Herbert Irving Comprehensive Cancer Center. This work was supported by the National Institutes of Health RO1 AR077152 to S. Kousteni and I.M., R56 AR054447 to S. Kousteni and I.M., R35 CA253126 to R.R. and the V Foundation for Cancer Research to S. Kousteni and I.M. Study in ATRA-treated patients' samples provided from Shanghai Hospital was supported by the National Natural Science Foundation of China (NSFC) Youth Program (Grants 82100162) allocated to N. Liu.

AUTHOR CONTRIBUTIONS

Conceptualization, I.M., A.R. and S. Kousteni; methodology, I.M. and S. Kousteni; formal analysis, I.M., S.M.R., A.W., J.Z., R.R., S.P., J.S., and S. Kousteni; data curation, B.J.C, J.P.B., and A.M.A; resources, A.M.A, J.G.J., E.B., C.M.W., X.F., R.P.S., N. Liu, C.L.,M.H., S. Kousteni, G.G.-M., and A.R.; investigation, I.M., R.L., B.B., A.C.-D., P.V., I.R., S.M.R., N. Liu, M.G.-D., K.F., J.H., R.A.A., A.L.C., and J.F.; writing - original draft, I.M. and S. Kousteni; writing - review and editing, I.M., S.M.R., and S. Kousteni; visualization, I.M.; supervision, I.M. and S. Kousteni; project administration, I.M. and S. Kousteni; funding acquisition, I.M. and S. Kousteni.

DECLARATION OF INTERESTS

S. Kousteni is inventor on the issued patent 14/760,026 to the Trustees of Columbia University in the City of New York related to ATRA and anti-Jagged1 work. S. Kousteni, A.R., A.M.A., and I.M. are co-inventors on the pending patent application PCT/US2014/011295 filed by the Trustees of Columbia University in the City of New York related to the ATRA and anti-Jagged1 work. X.F and SK are inventors on the pending patent application U.S. Serial No. 63/330,294 filed by AvantGen for JAGGED1 binding agents and uses thereof.

STAR★METHODS

Detailed methods are provided in the online version of this paper and include the following:

- KEY RESOURCES TABLE
- EXPERIMENTAL MODEL AND STUDY PARTICIPANT DETAILS
  - Patient samples and stratification
  - Mice
- METHOD DETAILS
  - Mice treatment
  - Isolation of the fully human D1 clone
  - Determining affinity of the D1 clone
  - Generation of the D1
  - Pharmacokinetic analysis of the D1 chimera
  - Blood test
  - Histological analysis
  - Flow cytometry
  - Whole exome sequencing
  - Cell culture and treatment
  - Immunofluorescence cell staining
  - Western blotting
  - RNA isolation, cDNA synthesis and qRT-PCR
  - RNA-seq
- QUANTIFICATION AND STATISTICAL ANALYSIS

SUPPLEMENTAL INFORMATION

Supplemental information can be found online at https://doi.org/10.1016/j.ccell.2025.03.007.

Received: April 15, 2024
Revised: September 14, 2024
Accepted: March 5, 2025
Published: March 27, 2025

REFERENCES

1. Kantarjian, H., Kadia, T., DiNardo, C., Daver, N., Borthakur, G., Jabbour, E., Garcia-Manero, G., Konopleva, M., and Ravandi, F. (2021). Acute

myeloid leukemia: current progress and future directions. Blood Cancer J. *11*, 41. https://doi.org/10.1038/s41408-021-00425-3.

2. Klepin, H.D., Rao, A.V., and Pardee, T.S. (2014). Acute myeloid leukemia and myelodysplastic syndromes in older adults. J. Clin. Oncol. *32*, 2541–2552. https://doi.org/10.1200/JCO.2014.55.1564.
3. Hellström-Lindberg, E., Tobiasson, M., and Greenberg, P. (2020). Myelodysplastic syndromes: moving towards personalized management. Haematologica *105*, 1765–1779. https://doi.org/10.3324/haematol.2020.248955.
4. Jaiswal, S., Fontanillas, P., Flannick, J., Manning, A., Grauman, P.V., Mar, B.G., Lindsley, R.C., Mermel, C.H., Burtt, N., Chavez, A., et al. (2014). Age-related clonal hematopoiesis associated with adverse outcomes. N. Engl. J. Med. *371*, 2488–2498. https://doi.org/10.1056/NEJMoa1408617.
5. Xie, M., Lu, C., Wang, J., McLellan, M.D., Johnson, K.J., Wendl, M.C., McMichael, J.F., Schmidt, H.K., Yellapantula, V., Miller, C.A., et al. (2014). Age-related mutations associated with clonal hematopoietic expansion and malignancies. Nat. Med. *20*, 1472–1478. https://doi.org/10.1038/nm.3733.
6. Shlush, L.I., Zandi, S., Mitchell, A., Chen, W.C., Brandwein, J.M., Gupta, V., Kennedy, J.A., Schimmer, A.D., Schuh, A.C., Yee, K.W., et al. (2014). Identification of pre-leukaemic haematopoietic stem cells in acute leukaemia. Nature *506*, 328–333. https://doi.org/10.1038/nature13038.
7. Genovese, G., Kähler, A.K., Handsaker, R.E., Lindberg, J., Rose, S.A., Bakhoum, S.F., Chambert, K., Mick, E., Neale, B.M., Fromer, M., et al. (2014). Clonal hematopoiesis and blood-cancer risk inferred from blood DNA sequence. N. Engl. J. Med. *371*, 2477–2487. https://doi.org/10.1056/NEJMoa1409405.
8. Busque, L., Patel, J.P., Figueroa, M.E., Vasanthakumar, A., Provost, S., Hamilou, Z., Mollica, L., Li, J., Viale, A., Heguy, A., et al. (2012). Recurrent somatic TET2 mutations in normal elderly individuals with clonal hematopoiesis. Nat. Genet. *44*, 1179–1181. https://doi.org/10.1038/ng.2413.
9. Jan, M., Snyder, T.M., Corces-Zimmerman, M.R., Vyas, P., Weissman, I.L., Quake, S.R., and Majeti, R. (2012). Clonal evolution of preleukemic hematopoietic stem cells precedes human acute myeloid leukemia. Sci. Transl. Med. *4*, 149ra118. https://doi.org/10.1126/scitranslmed.3004315.
10. Corces-Zimmerman, M.R., Hong, W.J., Weissman, I.L., Medeiros, B.C., and Majeti, R. (2014). Preleukemic mutations in human acute myeloid leukemia affect epigenetic regulators and persist in remission. Proc. Natl. Acad. Sci. USA *111*, 2548–2553. https://doi.org/10.1073/pnas.1324297111.
11. Kode, A., Manavalan, J.S., Mosialou, I., Bhagat, G., Rathinam, C.V., Luo, N., Khiabanian, H., Lee, A., Murty, V.V., Friedman, R., et al. (2014). Leukaemogenesis induced by an activating β-catenin mutation in osteoblasts. Nature *506*, 240–244. https://doi.org/10.1038/nature12883.
12. Raaijmakers, M.H.G.P., Mukherjee, S., Guo, S., Zhang, S., Kobayashi, T., Schoonmaker, J.A., Ebert, B.L., Al-Shahrour, F., Hasserjian, R.P., Scadden, E.O., et al. (2010). Bone progenitor dysfunction induces myelodysplasia and secondary leukemia. Nature *464*, 852–857. https://doi.org/10.1038/nature08851.
13. Zambetti, N.A., Ping, Z., Chen, S., Kenswil, K.J.G., Mylona, M.A., Sanders, M.A., Hoogenboezem, R.M., Bindels, E.M.J., Adisty, M.N., Van Strien, P.M.H., et al. (2016). Mesenchymal Inflammation Drives Genotoxic Stress in Hematopoietic Stem Cells and Predicts Disease Evolution in Human Pre-leukemia. Cell Stem Cell *19*, 613–627. https://doi.org/10.1016/j.stem.2016.08.021.
14. Schepers, K., Pietras, E.M., Reynaud, D., Flach, J., Binnewies, M., Garg, T., Wagers, A.J., Hsiao, E.C., and Passegué, E. (2013). Myeloproliferative neoplasia remodels the endosteal bone marrow niche into a self-reinforcing leukemic niche. Cell Stem Cell *13*, 285–299. https://doi.org/10.1016/j.stem.2013.06.009.
15. Schepers, K., Campbell, T.B., and Passegué, E. (2015). Normal and leukemic stem cell niches: insights and therapeutic opportunities. Cell Stem Cell *16*, 254–267. https://doi.org/10.1016/j.stem.2015.02.014.
16. Walkley, C.R., Olsen, G.H., Dworkin, S., Fabb, S.A., Swann, J., McArthur, G.A., Westmoreland, S.V., Chambon, P., Scadden, D.T., and Purton, L.E. (2007). A microenvironment-induced myeloproliferative syndrome caused by retinoic acid receptor gamma deficiency. Cell *129*, 1097–1110. https://doi.org/10.1016/j.cell.2007.05.014.
17. Dong, L., Yu, W.M., Zheng, H., Loh, M.L., Bunting, S.T., Pauly, M., Huang, G., Zhou, M., Broxmeyer, H.E., Scadden, D.T., and Qu, C.K. (2016). Leukaemogenic effects of Ptpn11 activating mutations in the stem cell microenvironment. Nature *539*, 304–308. https://doi.org/10.1038/nature20131.
18. Stoddart, A., Wang, J., Hu, C., Fernald, A.A., Davis, E.M., Cheng, J.X., and Le Beau, M.M. (2017). Inhibition of WNT signaling in the bone marrow niche prevents the development of MDS in the Apcdel/+ MDS mouse model. Blood *129*, 2959–2970. https://doi.org/10.1182/blood-2016-08-736454.
19. Lane, S.W., Sykes, S.M., Al-Shahrour, F., Shterental, S., Paktinat, M., Lo Celso, C., Jesneck, J.L., Ebert, B.L., Williams, D.A., and Gilliland, D.G. (2010). The Apcmin mouse has altered hematopoietic stem cell function and provides a model for MPD/MDS. Blood *115*, 3489–3497. https://doi.org/10.1182/blood-2009-11-251728.
20. Bhagat, T.D., Chen, S., Bartenstein, M., Barlowe, A.T., Von Ahrens, D., Choudhary, G.S., Tivnan, P., Amin, E., Marcondes, A.M., Sanders, M.A., et al. (2017). Epigenetically Aberrant Stroma in MDS Propagates Disease via Wnt/beta-Catenin Activation. Cancer Res. *77*, 4846–4857. https://doi.org/10.1158/0008-5472.CAN-17-0282.
21. Burnett, A.K., Milligan, D., Prentice, A.G., Goldstone, A.H., McMullin, M.F., Hills, R.K., and Wheatley, K. (2007). A comparison of low-dose cytarabine and hydroxyurea with or without all-trans retinoic acid for acute myeloid leukemia and high-risk myelodysplastic syndrome in patients not considered fit for intensive treatment. Cancer *109*, 1114–1124. https://doi.org/10.1002/cncr.22496.
22. Estey, E.H., Thall, P.F., Pierce, S., Cortes, J., Beran, M., Kantarjian, H., Keating, M.J., Andreeff, M., and Freireich, E. (1999). Randomized phase II study of fludarabine + cytosine arabinoside + idarubicin +/- all-trans retinoic acid +/- granulocyte colony-stimulating factor in poor prognosis newly diagnosed acute myeloid leukemia and myelodysplastic syndrome. Blood *93*, 2478–2484.
23. Schlenk, R.F., Lübbert, M., Benner, A., Lamparter, A., Krauter, J., Herr, W., Martin, H., Salih, H.R., Kündgen, A., Horst, H.-A., et al. (2016). All-trans retinoic acid as adjunct to intensive treatment in younger adult patients with acute myeloid leukemia: results of the randomized AMLSG 07-04 study. Ann. Hematol. *95*, 1931–1942. https://doi.org/10.1007/s00277-016-2810-z.
24. Milligan, D.W., Wheatley, K., Littlewood, T., Craig, J.I.O., and Burnett, A.K.; NCRI Haematological Oncology Clinical Studies Group (2006). Fludarabine and cytosine are less effective than standard ADE chemotherapy in high-risk acute myeloid leukemia, and addition of G-CSF and ATRA are not beneficial: results of the MRC AML-HR randomized trial. Blood *107*, 4614–4622. https://doi.org/10.1182/blood-2005-10-4202.
25. Schlenk, R.F., Fröhling, S., Hartmann, F., Fischer, J.T., Glasmacher, A., del Valle, F., Grimminger, W., Götze, K., Waterhouse, C., Schoch, R., et al. (2004). Phase III study of all-trans retinoic acid in previously untreated patients 61 years or older with acute myeloid leukemia. Leukemia *18*, 1798–1803. https://doi.org/10.1038/sj.leu.2403528.
26. Green, A.C., Kocovski, P., Jovic, T., Walia, M.K., Chandraratna, R.a.S., Martin, T.J., Baker, E.K., and Purton, L.E. (2017). Retinoic acid receptor signalling directly regulates osteoblast and adipocyte differentiation from mesenchymal progenitor cells. Exp. Cell Res. *350*, 284–297. https://doi.org/10.1016/j.yexcr.2016.12.007.
27. Lübbert, M., Grishina, O., Schmoor, C., Schlenk, R.F., Jost, E., Crysandt, M., Heuser, M., Thol, F., Salih, H.R., Schittenhelm, M.M., et al. (2020). Valproate and Retinoic Acid in Combination With Decitabine in Elderly Nonfit Patients With Acute Myeloid Leukemia: Results of a Multicenter, Randomized, 2 × 2, Phase II Trial. J. Clin. Oncol. *38*, 257–270. https://doi.org/10.1200/JCO.19.01053.

28. Lübbert, M., Rüter, B.H., Claus, R., Schmoor, C., Schmid, M., Germing, U., Kuendgen, A., Rethwisch, V., Ganser, A., Platzbecker, U., et al. (2012). A multicenter phase II trial of decitabine as first-line treatment for older patients with acute myeloid leukemia judged unfit for induction chemotherapy. Haematologica *97*, 393–401. https://doi.org/10.3324/haematol.2011.048231.

29. Soriano, A.O., Yang, H., Faderl, S., Estrov, Z., Giles, F., Ravandi, F., Cortes, J., Wierda, W.G., Ouzounian, S., Quezada, A., et al. (2007). Safety and clinical activity of the combination of 5-azacytidine, valproic acid, and all-trans retinoic acid in acute myeloid leukemia and myelodysplastic syndrome. Blood *110*, 2302–2308. https://doi.org/10.1182/blood-2007-03-078576.

30. Meier, R., Greve, G., Zimmer, D., Bresser, H., Berberich, B., Langova, R., Stomper, J., Rubarth, A., Feuerbach, L., Lipka, D.B., et al. (2022). The antileukemic activity of decitabine upon PML/RARA-negative AML blasts is supported by all-trans retinoic acid: in vitro and in vivo evidence for cooperation. Blood Cancer J. *12*, 122. https://doi.org/10.1038/s41408-022-00715-4.

31. Grishina, O., Schmoor, C., Döhner, K., Hackanson, B., Lubrich, B., May, A.M., Cieslik, C., Müller, M.J., and Lübbert, M. (2015). DECIDER: prospective randomized multicenter phase II trial of low-dose decitabine (DAC) administered alone or in combination with the histone deacetylase inhibitor valproic acid (VPA) and all-trans retinoic acid (ATRA) in patients >60 years with acute myeloid leukemia who are ineligible for induction chemotherapy. BMC Cancer *15*, 430. https://doi.org/10.1186/s12885-015-1432-5.

32. Wass, M., Göllner, S., Besenbeck, B., Schlenk, R.F., Mundmann, P., Göthert, J.R., Noppeney, R., Schliemann, C., Mikesch, J.-H., Lenz, G., et al. (2021). A proof of concept phase I/II pilot trial of LSD1 inhibition by tranylcypromine combined with ATRA in refractory/relapsed AML patients not eligible for intensive therapy. Leukemia *35*, 701–711. https://doi.org/10.1038/s41375-020-0892-z.

33. Tayari, M.M., Santos, H.G.D., Kwon, D., Bradley, T.J., Thomassen, A., Chen, C., Dinh, Y., Perez, A., Zelent, A., Morey, L., et al. (2021). Clinical Responsiveness to All-trans Retinoic Acid Is Potentiated by LSD1 Inhibition and Associated with a Quiescent Transcriptome in Myeloid Malignancies. Clin. Cancer Res. *27*, 1893–1903. https://doi.org/10.1158/1078-0432.CCR-20-4054.

34. Reikvam, H., Hovland, R., Forthun, R.B., Erdal, S., Gjertsen, B.T., Fredly, H., and Bruserud, Ø. (2017). Disease-stabilizing treatment based on all-trans retinoic acid and valproic acid in acute myeloid leukemia - identification of responders by gene expression profiling of pretreatment leukemic cells. BMC Cancer *17*, 630. https://doi.org/10.1186/s12885-017-3620-y.

35. Geoffroy, M.-C., Esnault, C., and de Thé, H. (2021). Retinoids in hematology: a timely revival? Blood *137*, 2429–2437. https://doi.org/10.1182/blood.2020010100.

36. Belhabri, A., Thomas, X., Wattel, E., Chelghoum, Y., Anglaret, B., Vekhoff, A., Reman, O., Dombret, H., Dhedin, N., Michallet, M., et al. (2002). All trans retinoic acid in combination with intermediate-dose cytarabine and idarubicin in patients with relapsed or refractory non promyelocytic acute myeloid leukemia: a phase II randomized trial. Hematol. J. *3*, 49–55. https://doi.org/10.1038/sj.thj.6200141.

37. Burnett, A.K., Hills, R.K., Milligan, D.W., Goldstone, A.H., Prentice, A.G., McMullin, M.F., Duncombe, A., Gibson, B., and Wheatley, K. (2010). Attempts to optimize induction and consolidation treatment in acute myeloid leukemia: results of the MRC AML12 trial. J. Clin. Oncol. *28*, 586–595. https://doi.org/10.1200/JCO.2009.22.9088.

38. Degos, L., and Wang, Z.Y. (2001). All trans retinoic acid in acute promyelocytic leukemia. Oncogene *20*, 7140–7145. https://doi.org/10.1038/sj.onc.1204763.

39. de Thé, H., Pandolfi, P.P., and Chen, Z. (2017). Acute Promyelocytic Leukemia: A Paradigm for Oncoprotein-Targeted Cure. Cancer Cell *32*, 552–560. https://doi.org/10.1016/j.ccell.2017.10.002.

40. de Thé, H., and Chen, Z. (2010). Acute promyelocytic leukaemia: novel insights into the mechanisms of cure. Nat. Rev. Cancer *10*, 775–783. https://doi.org/10.1038/nrc2943.

41. Cicconi, L., and Lo-Coco, F. (2016). Current management of newly diagnosed acute promyelocytic leukemia. Ann. Oncol. *27*, 1474–1481. https://doi.org/10.1093/annonc/mdw171.

42. Küley-Bagheri, Y., Kreuzer, K.-A., Monsef, I., Lübbert, M., and Skoetz, N. (2018). Effects of all-trans retinoic acid (ATRA) in addition to chemotherapy for adults with acute myeloid leukaemia (AML) (non-acute promyelocytic leukaemia (non-APL)). Cochrane Database Syst. Rev. *8*, CD011960. https://doi.org/10.1002/14651858.CD011960.pub2.

43. Schlenk, R.F., Weber, D., Krzykalla, J., Kindler, T., Wulf, G., Hertenstein, B., Salih, H.R., Südhoff, T., Krauter, J., Martens, U., et al. (2023). Randomized phase-III study of low-dose cytarabine and etoposide +/- all-trans retinoic acid in older unfit patients with NPM1-mutated acute myeloid leukemia. Sci. Rep. *13*, 14809. https://doi.org/10.1038/s41598-023-41964-y.

44. de Botton, S., Cluzeau, T., Vigil, C., Cook, R.J., Rousselot, P., Rizzieri, D.A., Liesveld, J.L., Fenaux, P., Braun, T., Banos, A., et al. (2023). Targeting RARA overexpression with tamibarotene, a potent and selective RARα agonist, is a novel approach in AML. Blood Adv. *7*, 1858–1870. https://doi.org/10.1182/bloodadvances.2022008806.

45. Nasr, R., Guillemin, M.-C., Ferhi, O., Soilihi, H., Peres, L., Berthier, C., Rousselot, P., Robledo-Sarmiento, M., Lallemand-Breitenbach, V., Gourmel, B., et al. (2008). Eradication of acute promyelocytic leukemia-initiating cells through PML-RARA degradation. Nat. Med. *14*, 1333–1342. https://doi.org/10.1038/nm.1891.

46. Kakizuka, A., Miller, W.H., Umesono, K., Warrell, R.P., Frankel, S.R., Murty, V.V., Dmitrovsky, E., and Evans, R.M. (1991). Chromosomal translocation t(15;17) in human acute promyelocytic leukemia fuses RAR alpha with a novel putative transcription factor, PML. Cell *66*, 663–674. https://doi.org/10.1016/0092-8674(91)90112-c.

47. de Thé, H., Lavau, C., Marchio, A., Chomienne, C., Degos, L., and Dejean, A. (1991). The PML-RAR alpha fusion mRNA generated by the t(15;17) translocation in acute promyelocytic leukemia encodes a functionally altered RAR. Cell *66*, 675–684. https://doi.org/10.1016/0092-8674(91)90113-d.

48. Easwaran, V., Pishvaian, M., Salimuddin, null, and Byers, S. (1999). Cross-regulation of beta-catenin-LEF/TCF and retinoid signaling pathways. Curr. Biol. *9*, 1415–1418. https://doi.org/10.1016/s0960-9822(00)80088-3.

49. Zhu, X., Wang, W., Zhang, X., Bai, J., Chen, G., Li, L., and Li, M. (2015). All-Trans Retinoic Acid-Induced Deficiency of the Wnt/β-Catenin Pathway Enhances Hepatic Carcinoma Stem Cell Differentiation. PLoS One *10*, e0143255. https://doi.org/10.1371/journal.pone.0143255.

50. Liu, J., Stevens, J., Rote, C.A., Yost, H.J., Hu, Y., Neufeld, K.L., White, R.L., and Matsunami, N. (2001). Siah-1 mediates a novel beta-catenin degradation pathway linking p53 to the adenomatous polyposis coli protein. Mol. Cell *7*, 927–936.

51. Xue, J., Chen, Y., Wu, Y., Wang, Z., Zhou, A., Zhang, S., Lin, K., Aldape, K., Majumder, S., Lu, Z., and Huang, S. (2015). Tumour suppressor TRIM33 targets nuclear β-catenin degradation. Nat. Commun. *6*, 6156. https://doi.org/10.1038/ncomms7156.

52. Chitalia, V., Shivanna, S., Martorell, J., Meyer, R., Edelman, E., and Rahimi, N. (2013). c-Cbl, a ubiquitin E3 ligase that targets active β-catenin: a novel layer of Wnt signaling regulation. J. Biol. Chem. *288*, 23505–23517. https://doi.org/10.1074/jbc.M113.473801.

53. McKeown, M.R., Corces, M.R., Eaton, M.L., Fiore, C., Lee, E., Lopez, J.T., Chen, M.W., Smith, D., Chan, S.M., Koenig, J.L., et al. (2017). Superenhancer Analysis Defines Novel Epigenomic Subtypes of Non-APL AML, Including an RARα Dependency Targetable by SY-1425, a Potent and Selective RARα Agonist. Cancer Discov. *7*, 1136–1153. https://doi.org/10.1158/2159-8290.CD-17-0399.

54. Glass, D.A., Bialek, P., Ahn, J.D., Starbuck, M., Patel, M.S., Clevers, H., Taketo, M.M., Long, F., McMahon, A.P., Lang, R.A., and Karsenty, G. (2005). Canonical Wnt signaling in differentiated osteoblasts controls

osteoclast differentiation. Dev. Cell *8*, 751–764. https://doi.org/10.1016/j.devcel.2005.02.017.

55. Solimini, N.L., Liang, A.C., Xu, C., Pavlova, N.N., Xu, Q., Davoli, T., Li, M.Z., Wong, K.-K., and Elledge, S.J. (2013). STOP gene Phactr4 is a tumor suppressor. Proc. Natl. Acad. Sci. USA *110*, E407–E414. https://doi.org/10.1073/pnas.1221385110.

56. Abou Chacra, L., Ghosn, M., Ghayad, E., and Honein, K. (2001). A case of pancreatitis associated with all-trans-retinoic acid therapy in acute promyelocytic leukemia. Hematol. J. *2*, 406–407. https://doi.org/10.1038/sj.thj.6200132.

57. Teng, H.-W., Bai, L.-Y., Chao, T.-C., Wang, W.-S., and Chen, P.-M. (2005). Acute pancreatitis during all-trans-retinoic acid treatment for acute promyelocytic leukemia in a patient without overt hypertriglyceridemia. Jpn. J. Clin. Oncol. *35*, 94–96. https://doi.org/10.1093/jjco/hyi027.

58. De, D., Nath, U.K., and Chakrabarti, P. (2017). Pancreatitis in Acute Promyelocytic Leukemia: Drug-induced or Differentiation Syndrome? Indian J. Med. Paediatr. Oncol. *38*, 371–373. https://doi.org/10.4103/ijmpo.ijmpo_36_16.

59. Hoshino, T., Hatsumi, N., Takada, S., Sakura, T., and Miyawaki, S. (2008). All-trans-retinoic acid as a possible cause of acute pancreatitis even in the absence of hypertriglyceridemia. Int. J. Hematol. *88*, 121–122. https://doi.org/10.1007/s12185-008-0116-1.

60. Di Martino, O., Niu, H., Hadwiger, G., Kuusanmaki, H., Ferris, M.A., Vu, A., Beales, J., Wagner, C., Menéndez-Gutiérrez, M.P., Ricote, M., et al. (2021). Endogenous and combination retinoids are active in myelomonocytic leukemias. Haematologica *106*, 1008–1021. https://doi.org/10.3324/haematol.2020.264432.

61. Zuber, J., Radtke, I., Pardee, T.S., Zhao, Z., Rappaport, A.R., Luo, W., McCurrach, M.E., Yang, M.-M., Dolan, M.E., Kogan, S.C., et al. (2009). Mouse models of human AML accurately predict chemotherapy response. Genes Dev. *23*, 877–889. https://doi.org/10.1101/gad.1771409.

62. Nair, A.B., and Jacob, S. (2016). A simple practice guide for dose conversion between animals and human. J. Basic Clin. Pharm. *7*, 27–31. https://doi.org/10.4103/0976-0105.177703.

63. Bankova, A.K., Pang, W.W., Velasco, B.J., Long-Boyle, J.R., and Shizuru, J.A. (2021). 5-Azacytidine depletes HSCs and synergizes with an anti-CD117 antibody to augment donor engraftment in immunocompetent mice. Blood Adv. *5*, 3900–3912. https://doi.org/10.1182/bloodadvances.2020003841.

64. Döhner, H., Estey, E., Grimwade, D., Amadori, S., Appelbaum, F.R., Büchner, T., Dombret, H., Ebert, B.L., Fenaux, P., Larson, R.A., et al. (2017). Diagnosis and management of AML in adults: 2017 ELN recommendations from an international expert panel. Blood *129*, 424–447. https://doi.org/10.1182/blood-2016-08-733196.

65. Greenberg, P.L., Tuechler, H., Schanz, J., Sanz, G., Garcia-Manero, G., Solé, F., Bennett, J.M., Bowen, D., Fenaux, P., Dreyfus, F., et al. (2012). Revised international prognostic scoring system for myelodysplastic syndromes. Blood *120*, 2454–2465. https://doi.org/10.1182/blood-2012-03-420489.

66. Chopin, M., Preston, S.P., Lun, A.T.L., Tellier, J., Smyth, G.K., Pellegrini, M., Belz, G.T., Corcoran, L.M., Visvader, J.E., Wu, L., and Nutt, S.L. (2016). RUNX2 Mediates Plasmacytoid Dendritic Cell Egress from the Bone Marrow and Controls Viral Immunity. Cell Rep. *15*, 866–878. https://doi.org/10.1016/j.celrep.2016.03.066.

67. Karsenty, G. (2008). Transcriptional control of skeletogenesis. Annu. Rev. Genomics Hum. Genet. *9*, 183–196. https://doi.org/10.1146/annurev.genom.9.081307.164437.

68. Singh, P., Mohammad, K.S., and Pelus, L.M. (2020). CXCR4 expression in the bone marrow microenvironment is required for hematopoietic stem and progenitor cell maintenance and early hematopoietic regeneration after myeloablation. Stem Cell. *38*, 849–859. https://doi.org/10.1002/stem.3174.

69. Shahnazari, M., Chu, V., Wronski, T.J., Nissenson, R.A., and Halloran, B.P. (2013). CXCL12/CXCR4 signaling in the osteoblast regulates the mesenchymal stem cell and osteoclast lineage populations. FASEB J. *27*, 3505–3513. https://doi.org/10.1096/fj.12-225763.

70. Eghbali-Fatourechi, G.Z., Lamsam, J., Fraser, D., Nagel, D., Riggs, B.L., and Khosla, S. (2005). Circulating osteoblast-lineage cells in humans. N. Engl. J. Med. *352*, 1959–1966.

71. Zhou, X. (2024). Decitabine Plus All-Trans Retinoic Acid Versus Decitabine Monotherapy for Myelodysplastic Syndromes with Excess Blasts: A Multicentre. Randomized Controlled Trial *144*, 663–664. (ASH).

72. Gu, C., Wang, R., Kang, H., He, X., Chen, J., Lin, Z., Liu, Y., Yang, T., Wu, D., and Han, Y. (2024). A prospective study of all-trans retinoic acid plus venetoclax and azacitidine in newly diagnosed acute myeloid leukemia. J. Clin. Orthod. *42*, 6545. https://doi.org/10.1200/JCO.2024.42.16_suppl.6545.

73. Bresser, H., Schmoor, C., Grishina, O., Pfeifer, D., Thomas, J., Rehman, U.-U., Crysandt, M., Jost, E., Thol, F., Heuser, M., et al. (2025). Impact of TP53 Mutation Status in Elderly AML Patients When Adding All-Trans Retinoic Acid or Valproic Acid to Decitabine. Eur. J. Haematol. *114*, 231–237. https://doi.org/10.1111/ejh.14304.

74. Papaemmanuil, E., Gerstung, M., Bullinger, L., Gaidzik, V.I., Paschka, P., Roberts, N.D., Potter, N.E., Heuser, M., Thol, F., Bolli, N., et al. (2016). Genomic Classification and Prognosis in Acute Myeloid Leukemia. N. Engl. J. Med. *374*, 2209–2221. https://doi.org/10.1056/NEJMoa1516192.

75. Papaemmanuil, E., Gerstung, M., Malcovati, L., Tauro, S., Gundem, G., Van Loo, P., Yoon, C.J., Ellis, P., Wedge, D.C., Pellagatti, A., et al. (2013). Clinical and biological implications of driver mutations in myelodysplastic syndromes. Blood *122*, 3616–3699. https://doi.org/10.1182/blood-2013-08-518886.

76. Cerami, E., Gao, J., Dogrusoz, U., Gross, B.E., Sumer, S.O., Aksoy, B.A., Jacobsen, A., Byrne, C.J., Heuer, M.L., Larsson, E., et al. (2012). The cBio cancer genomics portal: an open platform for exploring multidimensional cancer genomics data. Cancer Discov. *2*, 401–404. https://doi.org/10.1158/2159-8290.CD-12-0095.

77. Christiansen, D.H., Andersen, M.K., and Pedersen-Bjergaard, J. (2001). Mutations with loss of heterozygosity of p53 are common in therapy-related myelodysplasia and acute myeloid leukemia after exposure to alkylating agents and significantly associated with deletion or loss of 5q, a complex karyotype, and a poor prognosis. J. Clin. Oncol. *19*, 1405–1413. https://doi.org/10.1200/JCO.2001.19.5.1405.

78. Reilly, A., Busch, S., Abkowitz, J.L., Becker, P.S., and Doulatov, S. (2019). Deletions of 5q Promote Genome Instability in TP53-Mutant MDS/AML. Blood *134*, 1244. https://doi.org/10.1182/blood-2019-127038.

79. Volkert, S., Kohlmann, A., Schnittger, S., Kern, W., Haferlach, T., and Haferlach, C. (2014). Association of the type of 5q loss with complex karyotype, clonal evolution, TP53 mutation status, and prognosis in acute myeloid leukemia and myelodysplastic syndrome. Genes Chromosomes Cancer *53*, 402–410. https://doi.org/10.1002/gcc.22151.

80. Zhao, D., Eladl, E., Zarif, M., Capo-Chichi, J.-M., Schuh, A., Atenafu, E., Minden, M., and Chang, H. (2023). Molecular characterization of AML-MRC reveals TP53 mutation as an adverse prognostic factor irrespective of MRC-defining criteria, TP53 allelic state, or TP53 variant allele frequency. Cancer Med. *12*, 6511–6522. https://doi.org/10.1002/cam4.5421.

81. Pitel, B.A., Sharma, N., Zepeda-Mendoza, C., Smadbeck, J.B., Pearce, K.E., Cook, J.M., Vasmatzis, G., Sachs, Z., Kanagal-Shamanna, R., Viswanatha, D., et al. (2021). Myeloid malignancies with 5q and 7q deletions are associated with extreme genomic complexity, biallelic TP53 variants, and very poor prognosis. Blood Cancer J. *11*, 18. https://doi.org/10.1038/s41408-021-00416-4.

82. Rucker, F.G., Schlenk, R.F., Bullinger, L., Kayser, S., Teleanu, V., Kett, H., Habdank, M., Kugler, C.M., Holzmann, K., Gaidzik, V.I., et al. (2012). TP53 alterations in acute myeloid leukemia with complex karyotype correlate with specific copy number alterations, monosomal karyotype, and dismal outcome. Blood *119*, 2114–2121. https://doi.org/10.1182/blood-2011-08-375758.

83. Stahl, M., and Tallman, M.S. (2019). Differentiation syndrome in acute promyelocytic leukaemia. Br. J. Haematol. *187*, 157–162. https://doi.org/10.1111/bjh.16151.

84. Frankel, S.R., Eardley, A., Lauwers, G., Weiss, M., and Warrell, R.P. (1992). The "retinoic acid syndrome" in acute promyelocytic leukemia. Ann. Intern. Med. *117*, 292–296. https://doi.org/10.7326/0003-4819-117-4-292.

85. Montesinos, P., Bergua, J.M., Vellenga, E., Rayón, C., Parody, R., de la Serna, J., León, A., Esteve, J., Milone, G., Debén, G., et al. (2009). Differentiation syndrome in patients with acute promyelocytic leukemia treated with all-trans retinoic acid and anthracycline chemotherapy: characteristics, outcome, and prognostic factors. Blood *113*, 775–783. https://doi.org/10.1182/blood-2008-07-168617.

86. Xu, C., Xu, Z., Zhang, Y., Evert, M., Calvisi, D.F., and Chen, X. (2022). β-Catenin signaling in hepatocellular carcinoma. J. Clin. Investig. *132*, e154515. https://doi.org/10.1172/JCI154515.

87. Bian, J., Dannappel, M., Wan, C., and Firestein, R. (2020). Transcriptional Regulation of Wnt/β-Catenin Pathway in Colorectal Cancer. Cells *9*, 2125. https://doi.org/10.3390/cells9092125.

88. Xu, X., Zhang, M., Xu, F., and Jiang, S. (2020). Wnt signaling in breast cancer: biological mechanisms, challenges and opportunities. Mol. Cancer *19*, 165. https://doi.org/10.1186/s12943-020-01276-5.

89. Kocher, H.M., Basu, B., Froeling, F.E.M., Sarker, D., Slater, S., Carlin, D., deSouza, N.M., De Paepe, K.N., Goulart, M.R., Hughes, C., et al. (2020). Phase I clinical trial repurposing all-trans retinoic acid as a stromal targeting agent for pancreatic cancer. Nat. Commun. *11*, 4841. https://doi.org/10.1038/s41467-020-18636-w.

90. Reikvam, H., Hovland, R., Forthun, R.B., Erdal, S., Gjertsen, B.T., Fredly, H., and Bruserud, Ø. (2017). Disease-stabilizing treatment based on all-trans retinoic acid and valproic acid in acute myeloid leukemia – identification of responders by gene expression profiling of pretreatment leukemic cells. BMC Cancer *17*, 630. https://doi.org/10.1186/s12885-017-3620-y.

91. Schneider, C.A., Rasband, W.S., and Eliceiri, K.W. (2012). NIH Image to ImageJ: 25 years of image analysis. Nat. Methods *9*, 671–675. https://doi.org/10.1038/nmeth.2089.

92. Dempster, D.W., Compston, J.E., Drezner, M.K., Glorieux, F.H., Kanis, J.A., Malluche, H., Meunier, P.J., Ott, S.M., Recker, R.R., and Parfitt, A.M. (2013). Standardized nomenclature, symbols, and units for bone histomorphometry: a 2012 update of the report of the ASBMR Histomorphometry Nomenclature Committee. J. Bone Miner. Res. *28*, 2–17. https://doi.org/10.1002/jbmr.1805.

93. Kode, A., Mosialou, I., Manavalan, S.J., Rathinam, C.V., Friedman, R.A., Teruya-Feldstein, J., Bhagat, G., Berman, E., and Kousteni, S. (2016). FoxO1-dependent induction of acute myeloid leukemia by osteoblasts in mice. Leukemia *30*, 1–13. https://doi.org/10.1038/leu.2015.161.

94. Rached, M.-T., Kode, A., Xu, L., Yoshikawa, Y., Paik, J.-H., Depinho, R.A., and Kousteni, S. (2010). FoxO1 is a positive regulator of bone formation by favoring protein synthesis and resistance to oxidative stress in osteoblasts. Cell Metab. *11*, 147–160. https://doi.org/10.1016/j.cmet.2010.01.001.

95. Reinisch, A., Thomas, D., Corces, M.R., Zhang, X., Gratzinger, D., Hong, W.-J., Schallmoser, K., Strunk, D., and Majeti, R. (2016). A humanized bone marrow ossicle xenotransplantation model enables improved engraftment of healthy and leukemic human hematopoietic cells. Nat. Med. *22*, 812–821. https://doi.org/10.1038/nm.4103.

96. Veeman, M.T., Slusarski, D.C., Kaykas, A., Louie, S.H., and Moon, R.T. (2003). Zebrafish prickle, a modulator of noncanonical Wnt/Fz signaling, regulates gastrulation movements. Curr. Biol. *13*, 680–685. https://doi.org/10.1016/s0960-9822(03)00240-9.

97. Dobin, A., Davis, C.A., Schlesinger, F., Drenkow, J., Zaleski, C., Jha, S., Batut, P., Chaisson, M., and Gingeras, T.R. (2013). STAR: ultrafast universal RNA-seq aligner. Bioinformatics *29*, 15–21. https://doi.org/10.1093/bioinformatics/bts635.

98. Liao, Y., Smyth, G.K., and Shi, W. (2014). featureCounts: an efficient general purpose program for assigning sequence reads to genomic features. Bioinformatics *30*, 923–930. https://doi.org/10.1093/bioinformatics/btt656.

Please cite this article in press as: Mosialou et al., A niche driven mechanism determines response and a mutation-independent therapeutic approach for myeloid malignancies, Cancer Cell (2025), https://doi.org/10.1016/j.ccell.2025.03.007

STAR★METHODS

KEY RESOURCES TABLE

REAGENT or RESOURCE	SOURCE	IDENTIFIER
Antibodies		
PerCpCy5.5 anti mouse CD45	eBioscience	Cat#45-0451-80, Clone 30-F11; RRID: AB_906233
FITC anti mouse Ter119	Biolegend	Cat#116206, Clone TER119; RRID: AB_313707
PE anti mouse CD71	BD Biosciences	Cat#553267, Clone C2F2; RRID: AB_394744
PECy7 anti mouse CD41	eBioscience	Cat#25-0411, Clone MWReg30; RRID: AB_1234972
APC or FITC anti mouse CD11b	eBioscience	Cat#17-0112, Clone M1/70; RRID: AB_469342
v450 or PE anti mouse GR1	Invitrogen	Cat#12-5931, Clone RB6-8C5; RRID: AB_466044
PE anti mouse B220	eBioscience	Cat#12-0452 Clone RA3-6B2; RRID: AB_465670
FITC anti mouse CD19	eBioscience	Cat#11-0193, Clone 1D3; RRID: AB_657665
APC anti mouse CD4	BD Pharmingen	Cat#553051, Clone RM4-5; RRID:AB_398528
v450 anti mouse CD8a	BD Biosciences	Cat#560471, Clone53-6.7; RRID: AB_1645282
PerCpCy5.5 anti mouse Lineage antibody cocktail	BD Pharmingen	Cat#51-9006964, Clones 145-2C11, M1/70, RA3-6B2, TER-119, RB6-8C5; RRID: AB_10053179
APC anti mouse c-Kit	BD Pharmingen	Cat#553356, Clone 2B8; RRID: AB_398536
PECy7 anti mouse Ly6A/E	BD Biosciences	Cat#558162, Clone D7; RRID: AB_647253
APC-Cy7 anti mouse CD48	Biolegend	Cat#103432Clone HM48-1; RRID: AB_2561463
FITC anti mouse CD150	Invitrogen	Cat#11-1502-82, Clone mShad150; RRID: AB_11041521
PE anti mouse FcgRII/III	eBioscience	Cat#12-0161-82, Clone 93; RRID: AB_465568
FITC anti mouse CD34	eBioscience	Cat#11-0341-82, Clone RAM34; RRID: AB_465021
Pacific Blue anti human CD34	eBioscence	Cat#48-0349-42, Clone 4H1; RRID: AB_10733282
Alexa Fluor 700 anti human CD34	BD Biosciences	Cat#561440, Clone 581 (RUO); RRID: AB_10715443
FITC anti human JAG1	R&D	Cat#FAB1277F, Clone188331; RRID: AB_2128261
Pacific-blue-anti-human lineage antibody cocktail	BioLegend	Cat#348805, Clone RPA-2.10, OKT3, 61D3, CB16, HIB19, ULY56, HIR2; RRID: AB_2889063
APC anti human Runx2	Santa Cruz Biotechnology	Cat#sc-10758, clone M-70; RRID: AB_2184247
PECY7 anti human osteocalcin	Santa Cruz Biotechnology	Cat#sc-18319, clone V-19; RRID: AB_2064904
FITC anti human osteocalcin	Santa Cruz Biotechnology	Cat#sc-365797, clone G-5; RRID: AB_10859392

(*Continued on next page*)

Please cite this article in press as: Mosialou et al., A niche driven mechanism determines response and a mutation-independent therapeutic approach for myeloid malignancies, Cancer Cell (2025), https://doi.org/10.1016/j.ccell.2025.03.007

Continued

REAGENT or RESOURCE	SOURCE	IDENTIFIER
PE anti human activated (non-phosphorylated) b-catenin	Cell Signaling	Cat#13537S, clone D13A1 RRID: AB_2798251
PE anti human glycophorin-A	BD Biosciences	Cat#555570, clone GA-R2; RRID: AB_395949
FITC anti human Band 3	Miltenyi Biotec	Cat#130-119-780, clone RE A368; RRID: AB_2751838
APC anti human CD11b	Thermo Fisher Scientific	Cat#17-0118-42, clone ICRF44; RRID: AB_2016659
FITC anti human CD15	BD Pharmingen	Cat#560828, clone HI98; RRID: AB_10563612
β-Catenin	Cell Signaling	Cat#2677, clone L54E2; RRID: AB_1030943
b-catenin	Cell Signaling	Cat#9587; RRID: AB_10695312
HEY1	Abcam	Cat# ab154077; RRID: AB_2893447
Runx2	Abcam	Cat# ab192256; RRID: AB_2713945
Alexa fluor 488-conjugated secondary antibody	Life technologies	A11029; RRID: AB_2534088
Alexa fluor 488-conjugated secondary antibody	Thermo Fisher Scientific	A11034; RRID: AB_2576217
Alexa fluor 594-conjugated secondary antibody	Thermo Fisher Scientific	A11005; RRID: AB_2534073
goat anti-rabbit IgG H+L	Vectastain	BA-1000; RRID: AB_2313606
non-phospho, active β-catenin	Cell Signaling Technology	D13A1, Cat# 8814; RRID: AB_11127203
β-catenin	Cell Signaling Technology	Cat# 9562; RRID: AB_331149
GAPDH	Cell Signaling Technology	D16H11, Cat# 5174; RRID: AB_10622025
β-actin	Santa Cruz Biotechnology	C4, Cat# sc-47778; RRID: AB_2714189
histone H3	Cell Signaling Technology	D1H2, Cat# 4499; RRID: AB_10544537
Biological samples		
Bone marrow biopsies	M.D. Anderson Cancer Center part of the clinical trial NCT00326170	
	the Centre Hospitaller Lyon Sud, France	
	the First Affiliated Hospital, Naval Medical University, Shanghai, China approved by Shanghai Hospital Ethics Committee (Protocol Title: Leukemia Special Disease Cohort Database and Biobank Research. Ethics approval number: CHEC2022-076	
	Myelodysplastic Syndromes Center at New York Presbyterian-Columbia University Medical Center (IRB Protocol Numbers: AAAK3058, AAAF4107, AAAF2693, AAAU4817)	
	Memorial Sloan-Kettering Hospital reviewed under a research exempt waiver).	
	University of Pennsylvania	
Healthy BM aspirates and bone biopsies	Orthopedic Surgery Department at Columbia University, in collaboration with Dr. R. Shah (IRB protocol number: AAAR3184)	
Experimental models: Organisms/strains		
$\beta cat(ex3)_{osb}$	Dr. M M Taketo, University of New Mexico	
2.3Col1a(I)-Cre	Dr. Karsenty, CUMC, USA	
$RAR\alpha_{fl/fl}$	Dr. Pierre Chambon, INSERM, France	
C57BL/6J	Jackson Laboratory	JAX: 000664
$Tet2^{fl/fl}$	Jackson Laboratory	JAX: 017573
Vav1-iCre	Jackson Laboratory	JAX: 008610
Vav1-NUP98/HOXD13^{Tg}	Jackson Laboratory	JAX: 010505
$Trp53^{-/-}$ and $Trp53^{+/-}$	Jackson Laboratory	JAX: 002101
Chemicals, peptides, and recombinant proteins		
ATRA	Sigma	Cat #R2625
anti-JAG1 (D1) or IgG	AvantGen Inc	N.A.

(*Continued on next page*)

Please cite this article in press as: Mosialou et al., A niche driven mechanism determines response and a mutation-independent therapeutic approach for myeloid malignancies, Cancer Cell (2025), https://doi.org/10.1016/j.ccell.2025.03.007

Continued

REAGENT or RESOURCE	SOURCE	IDENTIFIER
Cytarabine	Sigma	Cat #C3350000
Doxorubicin	Sigma	Cat # D2975000
5-Azacytidine	StemCell Technologies	Cat# 72012
recombinant extracellular JAG1	Acrobiosystems	Cat # JA1-H52H9
Recombinant Human Jagged 2 Fc Chimera Protein, CF	R&D Systems	Cat #1726-JG-050
murine Jag1-ECD as an Fc-fusion protein	Creative Biomart	Cat# Jag1-381M
human DLL-1	Acrobiosystems	Cat # DLL1-H52H8
DLL-4	Sino Biological	Cat # 10171-H08H
human *JAG1*	Sino Biological	Cat # HG11648-ACG
human *JAG2*	Sino Biological	Cat# HG19075-UT
human DLL-1	Sino Biological	Cat# HG10171-ACG
Human DLL-4	Sino Biological	Ca t# HG10171-ACG
BLOXALL Blocking Solution	Vector Labs	SP-6000
Goat serum	Vectastain	S-1012-50
VECTASTAIN Elite ABC Reagent	Vectastain	PK-7100
DAB substrate	Vectastain	SK-4100
hematoxylin QS	Vector Labs	H-3404
Urea	Sigma-Aldrich	U5128
N,N,N′,N′-Tetrakis(2-Hydroxypropyl) ethylenediamine	Sigma-Aldrich	12262
Sucrose	Sigma-Aldrich	S7903
PVP	Sigma-Aldrich	P5288
triton X-100	Sigma-Aldrich	T8787
pork skin gelatin	Sigma-Aldrich	G1890
Donkey serum	Abcam	ab7475
DAPI	Sigma-Aldrich	D9542
Phalloidin-iFluor 647	Abcam	ab176759
Fluoromont-G	Invitrogen	00-4958-02
TruStain FcX mouse	Biolegend	101320
TruStain FCX human	Biolegend	422302
Fixation/Permeablization buffer	Invitrogen	00-5123-43
permeabilization buffer	Invitrogen	00-833356
EDTA	Sigma-Aldrich	E5134
MEM-Alpha	Corning	10-009-CV
RPMI	Thermo Fisher Scientific	30-2001
FBS	Gibco	10-082-147
GlutaMAX	Gibco	35-050-061
antibiotic-antimycotic	Corning	30-004-CI
L-glutamine	Gibco	25-030-149
sodium pyruvate	Gibco	MT25000CI
non-essential amino acids	Gibco	11-140-050
McCoy's 5A	Gibco	16-600-082
collagenase P	Roche	45-11249002001
Trypsin	Gibco	25200114
β-glycerol-phosphate	Sigma-Aldrich	50020
Ascorbic acid	Sigma-Aldrich	A92902
pooled human platelet lysate (pHPL)	New York Blood Center	N.A.
preservative-free heparin	BD	306423

(*Continued on next page*)

Please cite this article in press as: Mosialou et al., A niche driven mechanism determines response and a mutation-independent therapeutic approach for myeloid malignancies, Cancer Cell (2025), https://doi.org/10.1016/j.ccell.2025.03.007

Continued

REAGENT or RESOURCE	SOURCE	IDENTIFIER
Ficoll-Paque	Cytia	GE17-1440-02
StemSpan SFEM-II	StemCell Technologies	09605
HSC expansion cocktail	Miltenyi Biotec	130-100-843
StemSpan erythroid expansion supplement	StemCell	02692
StemSpan myeloid expansion supplement	StemCell	02693
PFA	Sigma-Aldrich	158127
PBS		21-040-CV
Tween-20	Sigma-Aldrich	P1379
donkey serum	Jackson ImmunoResearch	017-000-121
Lipofectamine 3000	Invitrogen	L3000015
pRL-CMV Renilla	Promega	E2261
Notch1 luciferase reporter	Addgene	41726
Mouse recombinant Wnt-3a	R&D	1324-WNP
Human recombinant Wnt-3a	R&D	5035-WNP
pCDNA3.1	Gift from Karsenty Gerard Columbia University	
TCF/LEF reporter	gift from Randall Moon	Addgene 12456
ON-TARGETplus non-targeting pool (si-scramble)	Dharmacon	D-001810-10-05
ON-TARGETplus siRNA-SMARTpool targeting *RARa*	Dharmacon	L-047625-02-0005
ON-TARGETplus siRNA-SMARTpool targeting *RARg*	Dharmacon	L- 040974-00-0005
ON-TARGETplus siRNA-SMARTpool targeting *Siah1*	Dharmacon	L-044891-01-0005
ON-TARGETplus siRNA-SMARTpool targeting *Trim33*	Dharmacon	L-063673-01-0005
ON-TARGETplus siRNA-SMARTpool targeting *c-Cbl*	Dharmacon	L-040165-01-0005
Lipofectamine RNAiMAX Reagent	Invitrogen	13778150
PowerUP SYBR Green Master Mix	Applied Biosystems	A25742
Trizol	Invitrogen	15596026
Viability dye e450, e660, or e780	Invitrogen	Cat# 65-0863-18, 65-0864-18, 65-0865-14
Critical commercial assays		
Lineage Cell Depletion Kit	MACS	130-092-211
T Cell Depletion kit	Miltenyi Biotec	130-094-973
B Cell Depletion kit	Miltenyi Biotec	130-090-862
AllPrep DNA/RNA Micro kit	Qiagen	80284
Venor™ GeM Mycoplasma Detection Kit	Sigma-Aldrich	MP0025
Click-iT Edu cell proliferation kit	Invitrogen	C10337
Edu	Invitrogen	C10632
AnnexinV-pacific blue/Sytox AADvanced	Invitrogen	A35136
Dual-Glo Luciferase assay system	Promega	E2920
Cell Signaling Technology Cell Fractionation kit	Cell Signaling	9038
Bio-Rad *DC* protein assay	Bio-Rad	500-0116
UbiTest–Magnetic TUBE Elution Kit	LifeSensors	UM414M
Quantikine mouse SOST immunoassay	R&D	MSST00

(*Continued on next page*)

Please cite this article in press as: Mosialou et al., A niche driven mechanism determines response and a mutation-independent therapeutic approach for myeloid malignancies, Cancer Cell (2025), https://doi.org/10.1016/j.ccell.2025.03.007

Continued

REAGENT or RESOURCE	SOURCE	IDENTIFIER
Mouse C-reactive protein/CRP elisa kit-Quantikine	R&D	MCRP00
Mouse pentraxin 2/SAP elisa kit-Quantikine	R&D	MPTX20
Experimental models: cell lines		
OCI-AML3	DSMZ	ACC-582 RRID: CVCM_1844
THP-1	DSMZ	ACC-16 RRID: CVCL_0006
MC3T3-E1 Subclone 4	ATCC	CRL2593
U2OS	ATCC	HTB-96
Kasumi	ATCC	CRL-2724, RRID: CVCL_0589
U937	ATCC	CRL-1593.2 RRID:CVCL_0007
Software and algorithms		
Prism v9.5.1	GraphPad	https://www.graphpad.com/
ForeCyt	Sartorius	https://www.sartorius.com/
Osteomeasure (XP v 1.2.0.3.)	Osteometrics	https://www.osteometrics.com/
FACS Diva software	BDS Bioscences	https://www.bdbiosciences.com/
FlowJo v.10.8.2	FlowJo Corp.	https://www.flowjo.com/
HiSeq Control		https://www.illumina.com/
Illumina bcl2fastq 2.17		https://www.illumina.com/
Multi Target Analysis module of IN Cell Investigator	GE Healthcare	
ImageJ	Schneider et al.[91]	https://imagej.nih.gov/ij/
Deposited data		
Exome sequencing data from ATRA-treated mice	This study	NCBI SRA ID: PRJNA967739
RNA-seq data from patients treated with ATRA-containing regimen	This study	GEO ID: GSE262907
RNA-seq data from patients treated with ATRA+TCP	Tayari et al.[33]	GEO ID: GSE151594
Expression profiling by array of patients' AML cells treated with ATRA+VPA	Reikvam et al.[34]	GEO ID: GSE106096
RNA-seq data from osteoblasts isolated from healthy donors and treated with Wnt3a+ATRA	This study	GEO ID: GSE277588
RNA-seq data from LSK cells isolated from $\beta cat(ex3)_{osb}$ mice and their WT littermates	This study	GEO ID: GSE277597
RNA-seq data from $CD34^+$ cells isolated from βcat^{high} and βcat^{low} AML patients	This study	GEO ID: GSE277103
Original Western blot images	This study	Mendeley data https://doi.org/10.17632/75jjmbkft7.1

EXPERIMENTAL MODEL AND STUDY PARTICIPANT DETAILS

Patient samples and stratification

Primary bone marrow (BM) aspirate samples, peripheral blood and bone biopsies from MDS and AML patients were obtained de-identified. All studies were approved by the individual Institutional Review Board of all participating Institutions, the Columbia University Medical Center Institutional Review Board (IRB Protocol Numbers: AAAK3058, AAAF4107, AAAF2693, AAAU4817 and AAAR3184), the Shanghai Hospital Ethics Committee (Protocol Title: Leukemia Special Disease Cohort Database and Biobank Research. Ethics approval number: CHEC2022-076) and the M.D. Anderson Cancer Center (MDACC) ethics committee. Informed written consent was obtained from all participants. Research was conducted in compliance with the declaration of Helsinki for collection and use of sample materials in research protocols, and in compliance with IRB regulations.

BM samples for initial assessment of β-catenin activation status in patients' osteoblasts and survival analysis were obtained from an Institutional Review Board (IRB)-approved tissue repository at the Myelodysplastic Syndromes Center at New York Presbyterian-Columbia University Medical Center (IRB protocol number: AAAF4107, AAAF2693, AAAU4817) and Memorial Sloan-Kettering

Please cite this article in press as: Mosialou et al., A niche driven mechanism determines response and a mutation-independent therapeutic approach for myeloid malignancies, Cancer Cell (2025), https://doi.org/10.1016/j.ccell.2025.03.007

Hospital (reviewed under a research exempt waiver). Median age of patients analyzed was 74y (range: 30, 74) for MDS, 65y (range: 21, 90) for *De Novo* AML and 72y (range: 47, 87) for sAML. Detailed description of patient's characteristics is provided in Table S1. The study populations reflected the populations usually seen at the clinics at Columbia University Medical Center. Those include 60% males, 40% females with 60% Caucasian, 30% Hispanic, 10% African Americans and Non-Hispanic. 3-10ml of BM aspirate were collected from the iliac crest of the back of the hip bone. This group of 305 MDS and AML patients shown in Figure 1A, was not treated with ATRA.

Bone marrow biopsies from ATRA-treated patients were provided from M.D. Anderson Cancer Center (part of the clinical trial NCT00326170), the Centre Hospitalier Lyon Sud, France, the First Affiliated Hospital, Naval Medical University, Shanghai, China (approved by Shanghai Hospital Ethics Committee (Protocol Title: Leukemia Special Disease Cohort Database and Biobank Research. Ethics approval number: CHEC2022-076) and the Myelodysplastic Syndromes Center at New York Presbyterian-Columbia University Medical Center (IRB Protocol Number: AAAK3058). Median age of ATRA-treated patients at diagnosis was 69y (range: 23, 75) and consisted of 67% males, 33% females, 66% White, 13% Hispanic, 13% Asian and 6% Black. Detailed description of patients' characteristics and treatment regimen is provided in Table S2.

Characteristics of patients treated with ATRA (45mg/m$^{2.}$)+TCP (20mg BID), (ClinicalTrials.gov no. NCT02273102), shown in Figure 1F, and ATRA (22.5mg/m^2 BID, D1D14) in combination with VPA+theophyllamine (D3-disease progression, dose guided by serum levels) (ClinicalTrials.gov no. NCT00175812), shown in Figure 1G, are provided in previous studies,[33,34] respectively. With the exception of one patient, shown in Figures 1O and 1P who was treated with ATRA monotherapy, in all other patients ATRA was administered in combination therapies as defined in the results section, figure legends and Table S2.

Activation of β-catenin in osteoblastic cells was determined by flow cytometric analysis, as described in detail in the flow cytometry section, and/or immunostaining of bone marrow biopsies as described in the histological analysis section below and[11]. Data derived from flow cytometry or immunohistochemistry have been extensively validated in our original study, in which we first described the relevance of this pathway in human disease.[11]There are marked differences in the severity and biology of the disease in terms of survival, genetics and risk category among MDS, AML and MDS transformed to AML patients. To normalize for such differences, median, quartiles and cut-offs for fraction of βcat^{high} patients were defined within each cohort (MDS, *De Novo*, sAML), for evaluating effects on survival, mutational and cytogenetic profile and ELN risk group. β-cat^{high} (characterized by a high fraction of osteoblasts with active β-catenin, belonging to the upper quartile (Q3) of its distribution in patients: $\geq$ 19.53 for MDS, $\geq$ 37.38 for *De Novo* AML and $\geq$ 30.5 for sAML. β-cat^{low}: Q1-Q2. Cut-off value used for re-stratification of patients in β-cat^{high} or β-cat^{low}, based on β-catenin levels in all AML patients analyzed or the entire cohort of MDS/AML patients was equal to 32.88 (median=20.75) or 26 (median=9.06), respectively. Patients, with non-detectable nuclear active β-catenin by histological analysis (β-catenin negative), were included in β-cat^{low}. Univariate and multivariate survival analysis (Cox regression analysis) was performed in a subset of patients for which data on all covariates tested were available (MDS, *n*=147; *De Novo* AML, *n*=77; sAML, *n*=31). In studies involving evaluation of the therapeutic efficacy of ATRA or D1 in patients' cells or for ATRA-treated patients, we defined the" pathological" cut-off value for β-catenin activity in osteoblasts that distinguishes MDS, AML and sAML from healthy subjects. This is equal to 11.14, equivalent to the 5% FDR of the exponential distribution of osteoblastic β-catenin followed in healthy subjects. If imposed by brute force, none of the healthy controls passed that range (maximum osteoblastic β-catenin activity observed in healthy subjects: 9.09). In these studies, the term β-catenin positive (βcat$_{osb}^{+}$) and β-catenin negative (βcat$_{osb}^{-}$) is used.

Immunostained pictures from some of the same patients we are showing in the current manuscript, were shown in our original publication of this pathway.[11] Those patients are noted in Table S1. Osteoblasts were identified by staining with RUNX2, an osteoblast-specific transcription factor and their characteristic cuboidal shape, lining the bone surface as defined by standard histomorphometry guidelines.[92] The number of osteoblasts per mm of bone surface was calculated. The number of osteoblasts counted depends on the size of the sample and the bio-/pathophysiological characteristics of the individual and for this study, the size of the biopsy allowed for counting of at least 100 osteoblasts per biopsy.

Healthy BM aspirates and bone biopsies were obtained from patients who had a planned elective hip or knee surgery from the Orthopedic Surgery Department at Columbia University, in collaboration with Dr. R. Shah (IRB protocol number: AAAR3184). Study population consisted of 33% males or 50% males for the *ex vivo* study with a median age of 64y (range: 51, 78) or 60y (range:51, 78), respectively (Tables S1 and S4).

Mice

Mice with constitutive activation of β-catenin in the osteoblastic lineage, *βcat(ex3)$_{osb}$*, were generated by crossing *βcat(ex3)$_{fl/fl}$* mice with *2.3Col1a(I)-Cre* mice expressing *Cre*[1] under the control of the osteoblast-specific 2.3kb proximal promoter of the mouse *alpha1(I)*collagen gene, as previously described.[11,93] In *βcat(ex3)$_{fl/fl}$* mice, exon 3, encoding for all serine and threonine residues required for β-catenin phosphorylation by glycogen synthase kinase 3β (GSK-3β), is flanked by *loxP* sites. *βcat(ex3)$_{fl/fl}$;RARα$_{fl/fl}$* mice were generated by sequentially crossing offspring derived from *βcat(ex3)$_{fl/fl}$* mice bred with *RARα$_{fl/fl}$* mice[81] (provided by Dr. Pierre Chambon, INSERM, France) until double homozygosity for the two alleles. *βcat(ex3)$_{fl/fl}$;RARα$_{fl/fl}$* mice were subsequently crossed with *RARα$_{fl/fl}$;2.3Col1a(I)-Cre* mice to generate the experimental mice *βcat(ex3)$_{osb}$;RARα$_{osb-/-}$* and their WT littermate controls, *βcat(ex3)$_{fl/+}$;RARα$_{fl/fl}$*. *RARα$_{fl/fl}$;2.3Col1a(I)-Cre* mice were generated by crossing *RARα$_{fl/fl}$* mice with *2.3Col1a(I)-Cre* mice. WT C57BL/6J (stock # 000664), *Tet2$^{fl/fl}$* (stock # 017573), *Vav1-iCre* (stock # 008610), *Vav1-NUP98/HOXD13^{Tg}* (stock # 010505) and *Trp53$^{-/-}$* (stock # 002101) were purchased from the Jackson Laboratory. All mice were on C57BL/6 background and were bred and maintained in specific-pathogen-free facilities under standard laboratory conditions (12h on/off) and temperature-controlled

Please cite this article in press as: Mosialou et al., A niche driven mechanism determines response and a mutation-independent therapeutic approach for myeloid malignancies, Cancer Cell (2025), https://doi.org/10.1016/j.ccell.2025.03.007

environment at Columbia University Medical Center. Food and water were available *ad libitum* and powdered diet was provided to $\beta cat(ex3)_{osb}$ mice as these mice lack teeth due to osteopetrosis. Male and female mice were analyzed indistinctly, as no differences were observed between them, and sex- and age-matched WT littermates were used as controls in all experiments. Because littermate group allocation was performed by animal genotype, it was not possible for investigators to be blinded to mice allocation during experiments. Blinding was applied during histological and flow cytometry analysis. Littermates of the same genotype were randomly assigned to experimental groups. No mice were excluded from the analysis unless clearly indicated. Mouse genotypes were determined by PCR; primer sequences are available upon request. All mouse experiments were approved by, and performed in accordance with, the Institutional Animal Care and Use Committee at Columbia University (Protocol Number AC-AABR3600).

METHOD DETAILS

Mice treatment

Mice treatments started when mice were 10-day old. ATRA (purchased from Sigma Cat# R2625) was resuspended in DMSO at 40mg/ml and further freshly diluted in corn oil and administered subcutaneously at 5mg/kg twice a week for the first two months and once a week thereafter for a total of 6 months. anti-JAG1 (D1) or IgG, developed from AvantGen Inc., were freshly diluted in sterile PBS and administered subcutaneously at 3mg/kg once a week for 3 months. Chemotherapy regimen consisted of five consecutives daily intraperitoneally (i.p.) doses of cytarabine (Sigma Cat# C3350000) (100mg/kg) along with doxorubicin (Sigma Cat# D2975000) for the first three days (3mg/kg) or five consecutives daily i.p. doses of cytarabine (50mg/kg) along with doxorubicin for the first three days (1.5mg/kg), as indicated. 5-AZA (StemCell Technologies Cat# 72012) was freshly diluted in sterile PBS and administered i.p. at 5mg/kg/day for 5 consecutive days. Non-irradiated 8-week-old C57BL/6J female mice injected intravenously with MLL/AF9-dsRed cells ($0.2x10^{\wedge 6}$ cells/mouse) were treated with ATRA or D1 (or vehicle) starting 1 week following MLL/AF9 cell transplantation with the same dosing schedule described above. Mice were monitored for health overall (activity, mobility, grooming, eating, hunched posture) and body weight gain and survival for the time length indicated. Mice were euthanized if body weight loss was greater than 20% or mice showed sign of distress and hind limb paralysis. Leukemia progression in MLL/AF9 transplanted mice was assessed by fluorescence (MLL/AF9 dsRed) using the IVIS-Spectrum Optical Imaging System (Caliper, Perkin Elmer). Mice were shaved to reduce light attenuation.

Isolation of the fully human D1 clone

The anti-JAG1 antibody clones were isolated from the screening of AvantGen's human antibody libraries displayed by yeast cells as described in a patent application (US 10,011,829).

The libraries were screened using labeled recombinant extracellular JAG1 domain encompassing residues Gln34 to Ser 1046 with a poly-His tag at the C-terminus (hereon referred to as JAG1-His) purchased from Acrobiosystems (Cat# JA1-H52H9). After a preliminary enrichment for antigen-binding antibody clones using magnetic bead activated cell sorting (MACS) and biotinylated JAG1-His, the libraries were further enriched by FACS, using progressively lower concentrations of JAG1-His where biotinylated antigen was alternated with Dylight-650 labeled antigen to minimize selection of binders against the biotin-streptavidin complex. After the final round of FACS, the harvested yeast cells were plated onto agar plates and individual clones seeded into individual well of a 96-well plate. After induction, the antibody-containing yeast culture supernatant of individual clones was tested for binding specificity to both recombinant human and murine JAG1 ECD by ELISA and to 293 cells expressing full-length human JAG1 as a GFP fusion protein to confirm binding to native protein. The top clones were then sequenced, the DNA inserts encoding the heavy and light chain variable regions were subcloned into full-length IgG4 mammalian heavy and light chain expression vectors, which were used to transfect ExpiCHO cells. The IgG was purified from filtered culture supernatants using Protein G column chromatography and quality determined to be >95% pure by reducing and non-reducing SDS-PAGE and by HPLC.

Determining affinity of the D1 clone

The binding activity of the D1 clone to the following Notch ligands was assessed first by ELISA. Human JAG1-His, human JAG2-ECD as an Fc-fusion protein (R&D Systems; Cat#1726-JG-050), murine Jag1-ECD as an Fc-fusion protein (Creative Biomart; Cat# Jag1-381M), human DLL-1 (Acrobiosystems, Cat# DLL1-H52H8) and DLL-4 (Sino Biological Cat# 10171-H08H) as His-tagged extracellular domains were each coated at 200 ng/well onto separate duplicate columns of a 96-well Immulon plate overnight at 4°C. After blocking with PBS plus 2% BSA, the wells were washed and a 5-fold serial dilution of the purified D1 clone ranging from 30 nM to 0.0004 nM (Jag1 coated wells) or 500 nM to 0.0064 nM (other Notch ligands) was added. After 30 minutes, bound antibody was detected with HRP-labeled goat anti-human kappa chain (Jackson Immunoresearch Labs, Cat# 109-135-098). OD readings were plotted against concentration and curve fitting and apparent Kd values determined using GraphPad software.

To assess relative binding affinities to native Notch ligands, genes encoding human *JAG1* (Sino Biological, Cat# HG11648-ACG), human *JAG2* (Sino Biological, Cat# HG19075-UT), human DLL-1 (Sino Biological, Cat# HG10171-ACG) and DLL-4 (Sino Biological, Cat# HG10171-ACG) were subcloned into a mammalian pCMV3-C-GFPSpark expression vector (Sino Biological) to enable expression levels to be compared by assessing GFP fluorescence. The resulting vectors were used to transiently transfect 293 cells using the FreeStyle™ 293 Expression System (ThermoFisher Scientific). On Day 2 post-transfection, when robust GFP expression was observed, cells were harvested and washed with ice cold PBS containing EDTA and 0.5% BSA (PBSM) and blocked for 45 min at 4°C with rotation. The cells were transferred to a 96-well plate (150,000 cells/well) and pelleted by centrifugation. They were then

Please cite this article in press as: Mosialou et al., A niche driven mechanism determines response and a mutation-independent therapeutic approach for myeloid malignancies, Cancer Cell (2025), https://doi.org/10.1016/j.ccell.2025.03.007

resuspended in PBSM containing a serial dilution of D1 ranging from each serially diluted from 100 nM to 0.0017 nM for binding to cells expressing JAG1 or from 500 nM to 0.0085 nM for binding to cells expressing JAG2, DLL-1 or DLL-4 and incubated for 1h at 4°C with rotation. After the incubation, the cells were washed three times with ice cold PBSM by centrifugation then resuspended in fresh buffer. The washed cell pellets were then resuspended and incubated in the dark, at 4°C with rotation in PBSM containing APC-labeled goat anti-human-kappa-IgG (Jackson ImmunoResearch Laboratories, Inc., Cat# 109-135-098) to detect bound D1. Bound APC fluorescence was analyzed using an IntelliCyt® iQue Screener PLUS and ForeCyt Software (Sartorius) and curve fitting and apparent KD values determined using GraphPad software. The level of GFP fluorescence provided a measure of fusion protein expression to confirm equal expression levels of the different Notch ligands by the transfected 293 cells.

Generation of the D1

The heavy chain variable region of the anti-human D1 clone was subcloned into an AvantGen vector carrying the CH1 through CH3 murine Fcγ1 constant region. The resulting vector was co-transfected with a vector carrying the D1 light chain with a murine kappa light chain constant region in a 500 mL culture of ExpiCHO cells and the secreted antibody purified by Protein G affinity chromatography. For this, the filtered culture medium was split into two, and each 250 ml aliquot loaded onto a 1.5 ml Protein G column and eluted with 0.1M Glycine, pH 3.0, and neutralized. The protein G purified IgG was then purified further by FPLC size exclusion chromatography (SEC) using a HiLoad 16/600 Superdex 200 pg column (Sigma-Aldrich, Cat#28-9893-35) on an AKTA Explorer with 50mM $NaPO_4$ pH 6.9, 150mM KCl as the elution buffer. Fractions corresponding to the main peak were collected. A 25µl aliquot of the pooled fractions was then analyzed on a Bioresolve SEC Mab column (7.8 × 300 mm, 2.5µm) on an Agilent 1200 Series HPLC system. This yielded monodisperse material with a purity of 99.4%. An aliquot of the purified material was then assessed for endotoxin content using the Limulus amoebocyte lysate (LAL) assay (ThermoFisher, Cat# 88282) performed according to the manufacturer's protocol to ensure endotoxin levels were well below the threshold for a biological effect (< 0.5EU/ml). The EU values for the Protein G purified D1 chimera were 0.035/mg (0.07/mL) and for the FPLC-SEC purified material 0.06/mg (0.12/mL) compared to 0.03 EU/mL for the isotype mouse IgG1 purchased from Crown Biosciences (Cat# CVP056, Lot #0820L205).

Pharmacokinetic analysis of the D1 chimera

Nine C57BL/6 female mice, 6-8 weeks old, were administered a single dose of 1,3 or 10 mg/kg D1 by subcutaneous injection on Day 0. The mice were divided into 3 groups of 3 and 100 µl blood sample were drawn via submandibular or facial vein using a lancet and placed in serum separator tubes from group 1 at 0.5 hr, 24 hr, and Day 7, from group 2 at 2hr, 48 hr, Day 14 and Day 21, and from group 3 at 4hr, 8 hr and 96 hr. Serum was stored at −80°C until analyzed for D1 content.

D1 concentrations were measured by ELISA as follows. Wells of a 96-well Immulon plate were coated with 135µl/well of 2ng/µl Jag-1-His solution overnight at 4°C then washed twice with PBS+2% BSA. For the calibration curve, the FPLC-SEC-purified D1-chimera clone or isotype control mouse IgG1 were added in a three-fold serial dilution ranging from 500 to 0.3 ng/ml in assay buffer (PBS buffer containing 2% BSA, 0.1% Tween20 plus 0.5% normal C57BL/6 female mouse serum (BioIVT, Cat #MSE01SRMX2N), total assay media volume of 100µl per well to duplicate wells, with assay buffer alone serving as background controls. A parallel duplicate set of wells was incubated in the same serial dilution of mouse isotype control IgG1. For the serum samples from the mice, a 1:200 and 1:600 dilution was added per well in triplicate. The wells were incubated for 1 hour (h) at room temperature (RT) with gentle rocking, washed briefly five times using a plate washer (Agilent, model Elx405) and bound mouse IgG detected by adding HRP-labeled goat anti-mouse kappa IgG (SouthernBiotech Cat. #1050-05) at a 1:5,000 dilution in PBS containing 2% BSA and 0.1% Tween 20, in a final volume of 100µl/well and incubating for 1h at RT with gentle rocking. Wells were then washed with TBS plus 1% Tween 20 and 100µl TBM (KPL SureBlue TMB Microwell Peroxidase Substrate; Seracare Life Sciences Inc #5120-0077) added. The reaction was quenched after approximately 500 seconds by adding 50µl/well 1M HCl and the absorbance at OD450 read with a Molecular Devices' Filter Max F5 plate reader. A standard curve was plotted after averaging and a best fit linear regression was calculated using Prism software. The R^2 for the linear fit of the standard curves was in the range 0.97 - 0.99. Antibody serum sample concentrations, which were also averaged, were calculated from the linear fit equation, and adjusted for dilution (1:200 or 1:600).

Blood test

Complete blood counts were assessed on cardiac-puncture peripheral blood collected at harvest/ endpoint into EDTA-coated tubes (Becton Dickinson) using a Genesis (Oxford Science) hematology system. For morphological assessment peripheral blood smears were stained with Wright Giemsa stain (Fisher Scientific Cat# NC9581034) and images were taken using an Olympus BX53F microscope. Blood chemistry was performed using a Heska Element DC Veterinary Chemistry Analyzer (Heska, Loveland, CO) at Columbia University's Institute of Comparative Medicine Diagnostic Laboratory. Serum levels of CRP (R&D, Cat# MCRP00), SAP (R&D, Cat# MPTX20) and sclerostin (R&D, Cat# MSST00) were determined by ELISA as per manufacturer's instructions. Serum was collected from cardiac puncture peripheral blood following 30min incubation at RT and centrifugation at 12.000rpm at 4°C.

Histological analysis

Freshly isolated mouse tibiae and spleens were fixed o/n in 10% neutral formalin, thoroughly washed with PBS, transferred to 70% ethanol, embedded in paraffin, sectioned at 5 µm and stained with H&E. Tibiae were decalcified in 14% EDTA pH7.4 for 7-14 days, depending on mice age, before transfer to 70% ethanol and embedding.

Please cite this article in press as: Mosialou et al., A niche driven mechanism determines response and a mutation-independent therapeutic approach for myeloid malignancies, Cancer Cell (2025), https://doi.org/10.1016/j.ccell.2025.03.007

CellPress

For immunohistochemical analysis, mice bones sections and patient's BM biopsies were rehydrated and washed in PBS prior to antigen retrieval at 60°C o/n in 10mM Tris-base, 1mM EDTA, 0.05% Tweeen-20, pH9. Subsequently, sections were washed in PBS, fixed for 5 min in 4%PFA, washed in PBS, blocked for 15min with BLOXALL Blocking Solution (Vector Labs SP-6000), washed in PBS, incubated with 2.5% normal blocking serum (goat) (Vectastain S-1012-50) for 20min and incubated o/n at 4°C with an antibody recognizing the C-terminus of β-catenin (Cell Signaling, Cat# 9587) or HEY1 (Abcam, Cat# ab154077) or RUNX2 (Abcam, Cat# ab192256), diluted in 1xPBS /2.5% normal serum. Next day, sections were washed with PBS and incubated for 1h with diluted secondary antibody solution (Vectastain BA-1000, goat anti-rabbit IgG H+L) 5ug/ml in 1xPBS containing 2% normal goat serum. Sections were then washed in PBS and incubated for 1h with VECTASTAIN Elite ABC Reagent (Vectastain PK-7100). After washing with PBS, sections were incubated with DAB substrate (Vectastain SK-4100), rinsed in water, counterstained with hematoxylin QS for 45sec (Vector Labs H-3404), rinsed in water and mounted.

For fluorescence and histochemical analysis of patient bone biopsies, sections were deparaffinized, rehydrated, and incubated in antigen retrieval solution as described above. Sections were subsequently blocked in 1xPBS containing 5% goat serum for 30 mins at RT and incubated o/n at 4°C with an antibody recognizing β-catenin (Cell Signaling, Cat# 2677) and RUNX2 (Abcam, Cat# ab192256), diluted in 1xPBS /5% goat serum. Next day, sections were washed with PBS and incubated for 1h with diluted secondary antibody solution (goat anti-rabbit IgG (H+L) Alexa Fluor 488 conjugate (Thermo Fisher Scientific, A11034) and goat anti-mouse IgG (H+L) Alexa Flor 594 (Thermo Fisher Scientific, A11005) in 1xPBS/5% goat serum. Sections were then washed, stained with DAPI (Sigma-Aldrich, Cat# D9542, dilution 1:1000) for 30 min at RT, washed with PBS and mounted with Fluoromont-G (Invitrogen, Cat# 00-4958-02) mounting medium. For analysis of mice tibiae and spleens, tissues were fixed o/n in ice-cold 4% paraformaldehyde (followed by decalcification for tibiae as above), thoroughly washed with ice-cold PBS and incubated for 24h (tibiae) or 8h (spleens) in PBS containing 10% urea (Sigma-Aldrich Cat# U5128), 15% N,N,N′,N′-Tetrakis(2-Hydroxypropyl) ethylenediamine (Sigma-Aldrich, Cat# 12262), 20% Sucrose (Sigma-Aldrich, Cat #S7903) and 2% PVP (Sigma-Aldrich, Cat #P5288) followed by incubation for 24h or 6h, respectively, in PBS containing 20% sucrose, 0,5% triton X-100 (Sigma-Aldrich, Cat #T8787) and 2% PVP. Subsequently, tissues were incubated at 60°C for 30 minutes in prewarmed embedding media (20% sucrose, 2% PVP and 8% pork skin gelatin (Sigma-Aldrich, Cat #G1890), embedded in disposable base mold, kept for 15 min at RT and then 1h at -20°C and sectioned at 50 μm thickness with a Leica cryostat. Sections were allowed to air-dry for 3h before storing at -20°C. For staining, sections were thawed at RT for 20 min, rehydrated in PBS for 10 min, incubated with 0.3% Triton X-100 for 10-20 min followed by incubation with donkey serum (Abcam, Cat# ab7475) for at least 5 min. Sections were then stained with DAPI (Sigma-Aldrich, Cat# D9542, dilution 1:1000) and Phalloidin-iFluor 647 Reagent (Abcam Cat# ab176759, 1:40) for 30 min at RT, washed with PBS and mounted with Fluoromont-G (Invitrogen, Cat# 00-4958-02) mounting medium. Sections were imaged with Zeiss LSM 710 confocal microscope and a Zeiss Axio Observer inverted fluorescence microscope. Images were processed with ImageJ (v1). For bone histomorphometry, three 5 μm bone sections from each mouse were stained with Von Kossa and toluidine blue for BV/TV and osteoblast quantification using Osteomeasure software (XP v 1.2.0.3.) from Osteometrics, and a Leica DMLB microscope outfitted with Sony DXC390 color video camera.

Flow cytometry

Single-cell suspensions of mouse bone marrow cells were incubated on ice for 20 min with conjugated antibodies in PBS containing 3 mM EDTA and 2.5 μg/ml TruStain FcX (Biolegend, Cat# 101320). The staining antibodies were purchased from Thermo Fisher Scientific, Biolegend or BD Biosciences, unless otherwise indicated, were conjugated with fluorescein isothiocyanate (FITC), Allophycocyanin (APC), phycoerythrin (PE), PE-Cy7, APC-Cy7, PerCP-Cyanine5.5 or Pacific Blue, and used at the indicated dilutions: CD45 (30-F11;1:300), Ter119 (TER119; 1:200), CD71 (C2F2;1:200), CD41 (MWReg30;1:100), CD11b (M1/70; 1:100), Gr1 (RB6-8C5; 1:100), B220 (RA3-6B2; 1:300), CD19 (1D3; 1:100), CD4 (RM4-5; 1:200), CD8a (53-6.7; 1:100), Lineage antibody cocktail (Lin) (145-2C11, M1/70, RA3-6B2, TER-119, RB6-8C5; 1:10), c-Kit (2B8; 1:50), Ly6A/E (D7;1:200), CD48 (HM48-1; 1:100), CD150 (mShad150; 1:25), FcγRII/III(93; 1:400) and CD34 (RAM34;1:50). For assessment of β-catenin activation status in primary patient's samples, single-cell suspensions of bone marrow or peripheral blood mononuclear cells were first stained for the cell surface markers by incubation for 20 min on ice with antibodies for CD34 (4H11 or 581; 1: 100), JAG1 (R&D, 188381;1:10) and the human hematopoietic lineage antibody cocktail (RPA-2.10, OKT3, 61D3, CB16, HIB19, ULY56, HIR2; 1:20) in PBS containing 3 mM EDTA and TruStain FcX (Biolegend, Cat# 422302; 1:20). Cells were then fixed using the Fixation/Permeabilization buffer (Invitrogen, Cat# 00-5123-43 diluted in #00-5223-56) for 30 min at RT, washed twice with permeabilization buffer (Invitrogen, Cat # 00-833356) and stained for the intracellular factors recognizing the osteoblastic lineage, as described before,[11] Runx2 (Santa Cruz Biotechnology, M-70; 1:100), osteocalcin (Santa Cruz Biotechnology, V-19 or G-5; 1:50) and activated (non-phosphorylated) β-catenin (Cell Signaling, D13A1; 1:50) for 30 min at RT. Following staining, cells were washed with PBS containing 2.5% fetal bovine serum (FBS), 2 mM EDTA (following prior wash with permeabilization buffer in case of intracellular staining) and sample acquisition was performed using LSRII or Fortessa cell analyzer and the FACS Diva software (BD Biosciences) or sort-purified using Influx Cell Sorter or Sony MA900 (BD Biosciences). Single color controls were used to set compensations and fluorescence minus one control were used to set gates. Analysis was performed with FlowJo v.10.8.2 (TreeStar) software. Cells were gated as shown in Figures S7E–K and as reported before.[11] In brief, cells were gated for size, shape and granularity using forward and side scatter parameters, SSC-a vs. FSC-A. Singlets were gated according to the pattern of FSC-H vs. FSC-A, followed by FSC-W vs. FSC-A. Dead cells were excluded by staining with Fixable Viability Dye (FVD) eFluor™ 450 (Invitrogen, Cat# 65-0863-18) or 780 (Invitrogen, Cat # 65-0865-14) or 506 (Invitrogen, Cat # 65-0866-14) (Thermo Fisher Scientific). Positive populations were determined by the specific antibodies, which were distinct from negative populations,

Please cite this article in press as: Mosialou et al., A niche driven mechanism determines response and a mutation-independent therapeutic approach for myeloid malignancies, Cancer Cell (2025), https://doi.org/10.1016/j.ccell.2025.03.007

single color controls and fluorescence minus one control. Osteoblastic lineage cells with active β-catenin were determined following the gating strategy shown in Figures S7E and S7K and,[11] by gating on osteoblastic lineage cells, $Runx2^+/Ocn^+$, following exclusion of hematopoietic lineage cells by gating on $CD34^-Lin^-$ cells.

Pre and post treatment samples for each patient were assessed at the same time. All samples from each individual center, (MD Anderson Cancer Center, Naval Medical University Shanghai, China and Centre Hospitalier Lyon Sud, France) were run together. The exact same antibody lots were used.

Whole exome sequencing

Genomic DNA from T(CD3) (Miltenyi Biotec Cat#130-094-973) and B cell (Miltenyi Biotec Cat#130-090-862) depleted mouse bone marrow cells or $CD3^+$ cells was isolated using AllPrep DNA/RNA Micro kit (Qiagen Cat# 80284) and quantified using Qubit 2.0 Fluorometer (ThermoFisher Scientific, Waltham, MA, USA). Enrichment probes were designed against the region of interest and synthesized through Twist Biosciences – Twist Mouse Exome Panel (South San Francisco, CA, USA). DNA library preparations and sequencing reactions were conducted at Azenta US (South Plainfield, NJ, USA). Briefly, the genomic DNA was fragmented by acoustic shearing with a Covaris S220 instrument. Fragmented DNAs were cleaned up and end repaired, as well as adenylated at the 3′ends. Adapters were ligated to the DNA fragments, and adapter-ligated DNA fragments were enriched with limited cycle PCR. Adapter-ligated DNA fragments were validated using Agilent TapeStation (Agilent Technologies, Palo Alto, CA, USA), and quantified using Qubit 2.0 Fluorometer. Adapter-ligated DNA fragments were hybridized with biotinylated baits. The hybrid DNAs were captured by streptavidin-coated binding beads. After extensive wash, the captured DNAs were amplified and indexed with Illumina indexing primers. Post-captured DNA libraries were validated using Agilent TapeStation (Agilent, Santa Clara, CA, USA) and quantified using Qubit 2.0 Fluorometer and Real-Time PCR (KAPA Biosystems, Wilmington, MA, USA). The sequencing libraries were multiplexed and clustered onto 1 lane of a flowcell. After clustering, the flowcell was loaded onto the Illumina HiSeq instrument according to manufacturer's instructions. The samples were sequenced using a 2x150bp Paired End (PE) configuration. Image analysis and base calling were conducted by the HiSeq Control Software (HCS). Raw sequence data (.bcl files) generated from Illumina HiSeq were converted into fastq files and de-multiplexed using Illumina bcl2fastq 2.17 software. One mismatch was allowed for index sequence identification.

Sequencing reads were mapped to the mouse mm10 genome build using bwa (v.0.7.17). Substitutions and indels were called using Strelka2 with default parameters; only variants with a mutant allele frequency of 5% or greater in tumors and 0% in normal, germline, control ($CD3^+$ cells) were included in analyses. The variant read count cutoff was 5 or more in tumor and depth was 20 or more in normal control. CNVs were analyzed using CNVkit 0.9.5 with parameters set to default. Segmentation was performed using circular binary segmentation.

Cell culture and treatment

OCI-AML3 cells (obtained from DSMZ Cat# ACC-582, RRID: CVCM_1844) were maintained in MEM-Alpha (Corning) supplemented with 20% heat inactivated FBS (Gibco), 1% GlutaMAX (Gibco) and 1% antibiotic-antimycotic (Corning). THP-1 cells (obtained from DSMZ Cat# ACC-16, RRID: CVCL_0006) were maintained in MEM-Alpha (Corning) supplemented with 10% heat inactivated FBS (Gibco), 1% GlutaMAX (Gibco) and 1% antibiotic-antimycotic (Corning). Kasumi-1 cells (obtained from ATCC Cat# CRL-2724, RRID: CVCL_0589) were maintained in RPMI 1640 (Thermo Fisher Scientific) supplemented with 20% heat inactivated FBS (Gibco), and 1% antibiotic-antimycotic (Corning). U937 cells (obtained from ATCC Cat# CRL-1583.2, RRID: CVCL_0007) were maintained in RPMI 1640 (Thermo Fisher Scientific) supplemented with 10% heat inactivated FBS (Gibco), and 1% antibiotic-antimycotic (Corning). MC3T3-E1 Subclone 4 (obtained from ATCC Cat# CRL2593) were maintained in MEM-Alpha (Corning) supplemented with 10% heat inactivated FBS (Gibco), 2mM L-glutamine (Gibco), 1mM sodium pyruvate (Gibco), 1x non-essential amino acids (Gibco) and 1% antibiotic-antimycotic (Corning). U2OS, human bone osteosarcoma cells (obtained from ATCC Cat# HTB-96) were maintained in McCoy's 5A Medium supplemented with 10% heat inactivated FBS (Gibco), 1% GlutaMAX (Gibco), and 1% antibiotic-antimycotic (Corning). Mouse primary osteoblasts were isolated as described previously.[94] In brief, mice calvaria of 2-3-day-old newborns were sequentially digested for 20, 40, and 90 min at 37°C in MEM-Alpha (Gibco) 10% FBS containing 0.1mg/ml of collagenase P (Roche) and 0.25% trypsin (Gibco). Cells of the first two digests were discarded, whereas cells released from the third digestion were cultured in MEM-Alpha (Corning) supplemented with 10% heat inactivated FBS (Gibco), 1% GlutaMAX (Gibco), 1x non-essential amino acids (Gibco) and 1% antibiotic-antimycotic (Corning). When cells reached confluence, medium was supplemented with 5mM β-glycerol-phosphate and 100μg/ml ascorbic acid (Sigma) to induce osteoblastic differentiation, which was replaced every 2 days thereafter for a total of 14 days. Primary human osteoblasts were obtained from explants of healthy patients undergoing hip/knee replacement surgery. Outgrowth cultures yielded osteoblastic stromal cells that were subsequently differentiated in osteogenic media (MEM-Alpha supplemented with 20% heat inactivated FBS, 1% GlutaMAX, 1x non-essential amino acids, 1% antibiotic-antimycotic, 5mM β-glycerol phosphate and 100 μg/ml ascorbic acid), that was changed every other day, for 14 days. Patient-derived bone marrow mesenchymal stem cells (BM-MSCs) were obtained from the outgrowth cultures of bone biopsies, as described above, or isolated and expanded from fresh bone marrow aspirates as described previously.[95] In brief, following wash with PBS, bone marrow aspirates were resuspended and cultured in MEM-Alpha supplemented with 10% pooled human platelet lysate (pHPL, New York Blood Center), 2U/ml preservative-free heparin and 1% antibiotic-antimycotic. After 24-48h non-adherent cells were removed by rinsing with PBS and adherent cells were further expanded with half-weekly medium changes until cells reached confluence. Patient-derived peripheral blood and bone marrow mononuclear cells, from freshly derived bone marrow aspirates, were isolated by density gradient centrifugation using Ficoll-Paque standard procedures. Bone marrow stem and progenitor cells were

Please cite this article in press as: Mosialou et al., A niche driven mechanism determines response and a mutation-independent therapeutic approach for myeloid malignancies, Cancer Cell (2025), https://doi.org/10.1016/j.ccell.2025.03.007

enriched using the Lineage Cell Depletion Kit (MACS Cat# 130-092-211) according to the manufacturer's protocol. Isolated Lin- cells were subsequently cultured under short-term expansion conditions in StemSpan SFEM-II (StemCell Technologies) supplemented with HSC expansion cocktail (Miltenyi Biotec, Cat# 130-100-843) and 100 I.U/ml penicillin/ 100μg/ml streptomycin for 3 days. All cells were cultured at 37°C in a 5% CO_2 atmosphere. Cell lines were tested routinely for mycoplasma using Venor™ GeM Mycoplasma Detection Kit (Sigma-Aldrich Cat# MP0025).

Co-cultures

Patient-derived lineage-depleted bone marrow mononuclear cells were co-cultured with their bone marrow mesenchymal stem cells (1.500 cells/well) in 384-well plates in the presence of 20nM D1 (or an isotype control) or 1μM ATRA (or vehicle, DMSO). Proliferating and dead cells were evaluated 24h later following staining with the Click-iT Edu cell proliferation kit (Invitrogen, Cat# C10337) and fixable Viability Dye eFluor™ 660 (Invitrogen, Cat# 65-0864-14). Effects on lineage determination were evaluated following co-culture of cells for 7 days under erythroid (StemSpan SFEM-II supplemented with StemSpan erythroid expansion supplement, StemCell, Cat# 02692) or myeloid differentiation (StemSpan SFEM-II supplemented with StemSpan myeloid expansion supplement, StemCell, Cat# 02693) conditions in the presence of 20nM D1 (or an isotype control) or 1μM ATRA (or vehicle, DMSO). Erythroid differentiation was assessed by quantification and calculation of percentage of total cells expressing glycophorin-A and Band 3 or percentage of total cells expressing CD11b and CD15 for myeloid lineage. For staining, cells were fixed in 4% PFA for 20 min at RT, washed three times with PBS supplemented with 5% Tween-20 (PBS-T), incubated with 2% normal donkey serum (Jackson ImmunoResearch, Cat# 017-000-121) in PBS-T for 30 min and subsequently incubated with the following conjugated antibodies (diluted 1:100 in PBS-T containing 2% normal donkey serum) for 2h at RT: glycophorin-A (BD, clone GA-R2); Band 3 (Miltenyi Biotec, clone REA368), CD11b (Thermo Fisher Scientific, clone ICRF44) or CD15 (Thermo Fisher Scientific, clone HI98). Following washes with PBS-T, cells were stained with DAPI for assessment of total cell numbers, washed with PBS-T and imaged using IN Cell Analyzer 2000 (GE Healthcare). Total number of cells and proportion of positive cells on each of the channels were calculated using the Image analysis algorithm that was developed using Multi Target Analysis module of IN Cell Investigator Software. Segmentation was done by imposing nuclear mask on every channel (FITC, dsRed and Cy5) and average intensity for each cell was calculated. Cells which had intensity above the background threshold were considered positive.

Apoptosis and proliferation assay

U2OS stably overexpressing human *JAG1* were plated in 12-well plate at a density of 0.1x10^6 cells/well in McCoy's 5a Medium (Gibco) supplemented with 10% FBS and 100 I.U/ml penicillin/ 100μg/ml streptomycin and cultured at 37°C in a 5% CO_2 atmosphere. Following day, media was removed and OCI-AML3 or THP-1 cells were overlayed at a density of 1x10^6 cells/ml in MEM-Alpha supplemented with 20% FBS and 100 I.U/ml penicillin/ 100μg/ml streptomycin, 1% GlutaMAX and 1% non-essential amino acids. Blocking antibodies or an isotype non-immune IgG control were added at increasing concentrations of 0.02, 0.06, 0.2, 0.6, 2, 6 and 20nM, diluted in PBS. 24h later, cell cycle/proliferation analysis was performed using the Click-iT Plus Edu Flow cytometry assay kit (following cell labeling with 10μM Edu for 2h at 37°C) (Invitrogen, Cat# C10632) and apoptotic cells were evaluated following staining with AnnexinV-pacific blue/Sytox AADvanced (Invitrogen, Cat# A35136), according to manufacturer's instructions. CD45 (Biolegend, clone HI30, 1:300 dilution or clone 2D1, dilution 1:100) was used for exclusion of any contaminating U2OS cells. Apoptotic or proliferating cells were determined in the gating population of CD45 positive cells by flow cytometry using BD Fortessa.

Notch1 luciferase reporter assay

6x10^6 U2OS cells (human bone osteosarcoma cell line) stably overexpressing *NOTCH1* were transiently transfected with 10μg of Notch1 luciferase reporter (4xCSL-Luc, gift from Raphael Kopan, Addgene plasmid #41726; RRID: Addgene_41726[84]), along with 50ng pRL-CMV Renilla (Promega) that serves as internal control, using Lipofectamine 3000 (Invitrogen). 8h later, cells were dissociated with enzyme-free cell dissociation buffer (Sigma Cat# C5914) and plated on white CoStar 96-well plates in co-culture with U20S cells stably overexpressing *JAG1* or the parental U2OS cell line at a density of 10.000 cells/well in McCoy's 5a Medium supplemented with 10% FBS and 100 I.U/ml penicillin/ 100μg/ml streptomycin. Blocking antibodies were added at increasing concentrations of 0, 0.02, 0.06, 0.2, 0.6, 2, 6 and 20nM in PBS. 24h later, luciferase activity was measured using Dual-Glo Luciferase assay system (Promega Cat# E2920) and quantified using Fluostar Omega (BMG Labtech Inc.). Luciferase activity was normalized to renilla activity and presented as the ratio of firefly to renilla. Control experiments were performed using a non-immune IgG antibody in co-culture with U2OS cells overexpressing *JAG1* or the U2OS parental cell line that do not overexpress *JAG1*.

ATRA treatment

Differentiated mouse and human primary osteoblasts or MC3T3-E1 cells were plated in their respective media supplemented with charcoal stripped fetal bovine serum (5% CSS), instead of FBS, and following day they were serum starved overnight in media supplemented with 0.5% CSS. Next day, cells were treated with 20ng/ml mouse (R&D, Cat# 1324-WNP) or human (R&D, Cat# 5035-WNP) recombinant Wnt-3a (or vehicle, PBS 0.1% BSA) for 3h and subsequently treated with 1μM ATRA (Sigma, Cat# R2625) (or vehicle, DMSO) for an additional 3h prior to sample collection for further analysis. For proteasome inhibition, cells were pre-treated with 10 μM MG-132 (Sigma # M7449) for 2h before ATRA treatment.

Gene silencing, overexpression and reporter assays

For gene overexpression studies, MC3T3-E1 cells were plated at a density of 0.3x10^6 cells/well and next day, cells were transfected with 200ng of a pCDNA3.1 expression vector encoding for wild type or a constitutive active mutant form of β-catenin[54] (gift from Dr. Karsenty Lab, Columbia University) or an empty vector control using Lipofectamine 3000 (Invitrogen), according to manufacturer's instructions. For luciferase reporter assays, MC3T3-E1 cells were plated on white CoStar 96-well plates at a density of 0.01x10^5 cells/well. Following day, cells were transiently transfected with 30ng TCF/LEF reporter (M50 Super 8xTOPFlash, gift from Randall

Please cite this article in press as: Mosialou et al., A niche driven mechanism determines response and a mutation-independent therapeutic approach for myeloid malignancies, Cancer Cell (2025), https://doi.org/10.1016/j.ccell.2025.03.007

Moon, Addgene plasmid #12456; RRID:Addgene_12456)[96] along with 60 ng of the pCDNA3.1 expression vector encoding for wild type or a constitutive active mutant form of β-catenin or the empty vector control and 1ng pRL-CMV Renilla (Promega) that was used as an internal control. Cells were subsequently serum starved overnight (0.5% CSS), treated with 1μM ATRA or vehicle and collected for RNA isolation and gene expression analysis or luciferase reporter assays 24h later. For luciferase assays upon Wnt-3a stimulation, following overnight starvation in 0.5% CSS, cells were treated with 20ng/ml recombinant Wnt-3a (or vehicle) for 3h, followed by treatment with 1μM ATRA (or vehicle) for 3h. Luciferase activity was determined using the Dual-Glo Luciferase Assay System (Promega) and quantified using Fluostar Omega. Luciferase activity was normalized to renilla activity and is presented as relative luciferase activity over vehicle-treated cells. For gene silencing, cells were transiently transfected with 100nM ON-TARGETplus non-targeting pool (si-scramble) (Dharmacon, Cat# D-001810-10-05) or ON-TARGETplus siRNA-SMARTpool targeting *RARα* (Dharmacon, Cat# L-047625-02-0005) or *RARγ* (Dharmacon, Cat# L- 040974-00-0005) or *Siah1* (Dharmacon, Cat# L-044891-01-0005) or *Trim33* (Dharmacon, Cat# L-063673-01-0005) or *c-Cbl* (Dharmacon, Cat# L-040165-01-0005) using Lipofectamine RNAiMAX Reagent (Invitrogen) according to manufacturer's instructions. Next day, cells were serum starved overnight (0.5% CSS) and subsequently treated with 20ng/ml recombinant Wnt-3a (or vehicle) for 3h, followed by treatment with 1μM ATRA (or vehicle) for 3h, as described above, prior to RNA isolation and gene expression analysis. In both cases, transfection efficiency was tested by real-time PCR.

Immunofluorescence cell staining

MC3T3-E1 cells were grown over 12mm glass coverslips, differentiated and treated with Wnt-3a and ATRA as described above, fixed in 4% PFA for 15 min at RT, permeabilized with PBS 0.3% Triton X-100 for 15min at RT, blocked in PBS supplemented with 5% normal goat serum (Jackson ImmunoResearch Cat# 005-000-121) and 0.3% Triton X-100 for 1h and subsequently incubated for 90min at RT with an antibody recognizing endogenous levels of total β-catenin (Cell Signaling, clone L54E2, 1:200 dilution). Following washes, samples were incubated with Alexa fluor 488-conjugated secondary antibody (Life technologies, Cat# A11029) for 2h, counterstained with DAPI, mounted with Fluoromont-G (Invitrogen, Cat# 00-4958-02) mounting medium and visualized using Zeiss Axio Observer inverted fluorescence microscope. Images were analyzed with ImageJ software (v1).

Western blotting

Following cell treatment as described above, nuclear and membrane protein extracts were purified using the Cell Signaling Technology Cell Fractionation kit (Cat# 9038), according to manufacturer's instructions. Protein concentration was determined with the Bio-Rad *DC* protein assay (Cat# 500-0116) and equivalent amounts of protein were resolved on SDS-polyacrylamide gel, transferred to a nitrocellulose membrane and probed with the following antibodies: non-phospho, active β-catenin (Cell Signaling Technology, D13A1, Cat# 8814), GAPDH (Cell Signaling Technology, D16H11, Cat# 5174), β-actin (Santa Cruz Biotechnology, C4, Cat# sc-47778) and histone H3 (Cell Signaling Technology, D1H2, Cat# 4499) following standard procedures. β-catenin ubiquitination was assessed using the UbiTest-Magnetic TUBE Elution Kit (LifeSensors Inc. Cat #UM414M) following the manufacturer's instructions. In brief, cells were lysed using RIPA lysis buffer supplemented with protease inhibitor and PR-619 (20uM) to further inhibit ubiquitin proteases. One sixth of total lysate was saved as input and the rest was used in the pull down. Pull down of total ubiquitinated proteins was achieved using a magnetic resin bead conjugated with a TUBE (tandem ubiquitin binding entities). Ubiquitinated substrates were eluted, and half was treated with a deubiquitinase (DUB). Ubiquitination can result in ineffective antibody recognition requiring DUB treatment for visualization on immunoblots. Proteins were analyzed by Western blotting using an antibody recognizing total β-catenin (Cell Signaling Technology, Cat# 9562).

RNA isolation, cDNA synthesis and qRT-PCR

RNA isolation, cDNA preparation and real-time PCR analyses were carried out following standard protocols. For bone tissue analysis, bone marrow cells were removed completely by extensively flushing the femurs with PBS. Trizol reagent was used for RNA extraction or the AllPrep DNA/RNA Micro kit (Qiagen Cat# 80284) for RNA extraction from sort-purified cells. Random hexamers cDNA synthesis kit (Clontech Laboratories) was used for reverse transcription PCR and PowerUP SYBR Green Master Mix (Applied Biosystems) for quantitative PCR. Primer sequences used are as follows: *Axin2* F: 5- 5'-caagcctggctccagaagat-3', R: 5'-gatcctgccttcgtacatgg-3'; *Lef1* F: 5'-tcatcacctacagcgacgag-3', R: 5'-gggtagaaggtggggatttc-3'; *Jag1* F: 5'-gaaatacacgtggccatctc-3', R: 5'-agacagagctcagcagagga-3'; *Tcf1* F: 5'-gccagaagcaaggagttcac-3', R: 5'- tacaccagatcccagcatca-3'; *Tcf3* F: 5'-ctcccttcctcggtgtatcc-3', R: 5'-ctaggcgtactccagagctc-3'; *Ctnnb1* F: 5'-caatggcttggaatgagactgc-3', R: 5'- ctcatgctccatcatagggtcc-3'; *RARα* F: 5'-cactgaaagtctacgtccggaa-3', R: 5'-ccctcagagttctccagcattt-3'; *RARβ* F: 5'-gaaaatcacagatctccgcagc-3', R: 5'-ctgactgactccactgttctcc-3'; *RARγ* F: 5'-tgacaagtcttctggctaccac-3', R: 5'- catgcccacttcgaaacacttt-3'; *Hes1* F: 5'-gccaatttgcctttctcatc-3', R: gagaggtgggctagggactt-3'; *Hes5* F: 5'-gcagcatagagcagctgaag-3', R: 5'-tagtcctggtgcaggctctt-3'; *Hey1* F: 5'- ggtacccagtgcctttgaga-3', R: 5'-agctcagataacgggcaac-3'; Cdkn1a F: 5'- *ctgtttctgtaacatcctggtctg-3', R: 5'-tcgagaagtatttattgagcacca-3'; Pram1 F: 5'-ggacttccgaaacctccaagc-3', R: 5'-ctgctcacttaactcagtctgtg-3'; Dhrs3 F: 5'- tgaaaaatgcctcaaggagacg-3', R: 5'- ggccatctggtacacctcttc-3'; Actb* F: 5'- gacctctatgccaacacagt-3', R: 5'- agtacttgcgctcaggagga-3'. For human samples: *AXIN2* F: 5'-ggttctggctatgtctttgcac-3', R: 5'-gcatttctctctggagctgttt-3'; *LEF*1 F: 5'-tgctagagacgctgatccataa-3', R: 5'-tgctagcattctcatgtgcttt-3'; *JAG1*; 5'- aggagatgatgtcaccaggtct-3', R: 5'-tcccatcatcccgtatatcttc-3'; *TCF1* F: 5'-tctctggcttctactccctgac-3', R: 5'-ctctgcttgtgtcttcaggttg-3'; *CDKN1A* F: 5'- cctggtgatgtccgacctg-3', R: 5'-ccatgagcgcatcgcaatc-3'; *PRAM1* F: 5'- cgaccccaacgctaagacac-3', R: 5'- gcacgtagccatatttgcctt-3'; *DHRS3* F: 5'- actgagtgccattacttcatctg-3', R: 5'-catcactgtccattaggctcttc-3'; *TGM2* F; 5'-gaggagctggtcttagagagg-3', R: 5'-cggtcacgacactgaaggtg-3'; *RARα* F: 5'-acaagaagaagaaggaggtgcc-3', R: 5'-gtcaatgtccagagagacacgt-3'; *RARγ* F: 5'-ccccaccccaatgcctctag-3', R: 5'-attggaaggggtggggagag-3';

Please cite this article in press as: Mosialou et al., A niche driven mechanism determines response and a mutation-independent therapeutic approach for myeloid malignancies, Cancer Cell (2025), https://doi.org/10.1016/j.ccell.2025.03.007

HES1 F: 5'-tctacctctctccttggtcctg-3', R: 5'-tatcagctggcattttcctttt-3'; *HES5* F: 5'-atcttctgccaagtgtctgacc-3', R: 5'-gccctgaagaa agtcctctaca-3'; *HEY1* F: 5'-gttggtggaaaggaaactgaag-3', R: 5'-ctcgcacaccatgatcacttat-3'; *HEY2* F: 5'-gggacagaagtcttgcaatagg-3', R: 5'- tgcactgctaaatgtcacctct-3'; *GAPDH* F: 5'-aatcccatcaccatcttccagg-3', R: 5'-tgctgatgatcttgaggctgtt-3'. *Actb* and *GAPDH* were used as internal controls for mouse and human samples, respectively. Data are presented as fold change over control (vehicle) after normalization with *Actb* or *GAPDH* levels.

RNA-seq

RNA from patients' $CD34^+$ cells or LSK cells from mice BM was extracted using the AllPrep kit (Qiagen). RNA from primary human osteoblasts treated with Wnt3a and ATRA or BMMNCs from ATRA-treated patients, pre and post treatment, was extracted using Trizol. RNA libraries were prepared using the Illumina TruSeq Stranded Total RNA kit, using a modified protocol by replacing the Illumina TruSeq PCR reaction with KAPA HiFi HotStart Ready Mix for the final PCR step to make it compatible with the Element Aviti. Roche Riboerase v2.17 reagent was used for samples from ATRA treated patients. Sequencing of libraries was done on a NovaSeq 6000 at Columbia Genome Center or Shanghai Hospital (for ATRA treated patients). 2x75 PE sequencing was performed. Reads were aligned to the human reference genome (Ensembl (RRID:SCR_002344) (hg38/GRCh38) or the mouse (version mm10) reference genome using the default settings in STAR aligner.[97] Read count values were extracted using featureCounts[98] and normalized gene expression were calculated as TPM (Transcripts Per Million). Differential expression analysis was performed by DEseq2 (RRID:SCR_015687). Log transformed plus-one TPM values were quantile normalized across samples. The normalized values were taken back to exponential, and the average expression value for each gene across each experimental group was calculated, based on which log2 fold change was calculated. Wilcoxon's rank sum test was applied to calculate p-values, followed by Benjamini-Hochberg adjustment. Genes were sorted based on log2 fold changes and the order was input to GSEA. MSigDB database C5 was taken as the category. For comparison of the expression profile between patients and mice samples, mouse gene symbols were converted to their orthologs in human for GSEA analysis. A total of 146 GO_BP terms with adjusted p-values < 0.05 in either AML patients or mice, was identified, broken down into four groups based on normalized enrichment scores (NES): positive in both AML patients and $\beta cat(ex3)_{osb}$ mice (n= 65), positive in AML patients and negative in $\beta cat(ex3)_{osb}$ mice (n= 23), negative in AML patients and positive in $\beta cat(ex3)_{osb}$ mice (n= 22) and negative in both AML patients and $\beta cat(ex3)_{osb}$ mice (n= 36). Fisher's exact test on these counts indicated significant co-occurrence of positive or negative NES between AML patients and $\beta cat(ex3)_{osb}$ mice (odds ratio = 4.57, p-value = 2.79e-5).

QUANTIFICATION AND STATISTICAL ANALYSIS

Results are reported as mean ± standard error of the mean (S.E.M.). Data assumed normal distribution, therefore unpaired, two-tailed Student's *t*-test was performed for comparisons between two groups and one- or two-way ANOVA for more than two groups' comparisons, as stated in the figure legends. All statistical tests were performed with GraphPad Prism v.9 software or Excel (Microsoft). *P* values of less than 0.05 were considered to be significant. Exact *P* values and sample size *(n)* are indicated in the figures and figure legends, respectively. Animal sample size estimates were determined using power analysis (power=80% and a=0.05) based on the mean and standard deviation from our previous studies. All single data points in all figures represent biological replicates, from separate mice, separate experiments (cell lines) or, in the case of primary cultures of human or murine osteoblasts, measurements were performed on independently grown cultures. In the case of human data, each data point corresponds to an independent patient sample. Replication of experiment details are found in each figure legend.

Gene expression matrices from ATRA clinical trials were downloaded from GSE151594 and GSE106096. Normalized Enrichment Score (NES) was calculated using R package GSVA for each pair of sample and NOTCH signature (https://www.gsea-msigdb.org/gsea/msigdb/cards/HALLMARK_NOTCH_SIGNALING). Then, the difference of NES between different groups was evaluated by *t*-test. In the case of merging two different datasets, quantile normalization was used to correct the batch effect before gene set enrichment analysis.